

Review

Recent Advances in Continuous MOF Membranes for Gas Separation and Pervaporation

Xiao Xu ^{1,2,*} , Yusak Hartanto ^{1,2} , Jie Zheng ³ and Patricia Luis ^{1,2,*} 

- ¹ Materials and Process Engineering (iMMC-IMAP), UCLouvain, Place Sainte Barbe 2, 1348 Louvain-la-Neuve, Belgium
- ² Research and Innovation Centre for Process Engineering (ReCIPE), Place Sainte Barbe 2, bte L5.02.02, 1348 Louvain-la-Neuve, Belgium
- ³ School of Chemistry and Chemical Engineering, Chongqing University, No. 55 Daxuecheng South Rd., Shapingba, Chongqing 401331, China
- * Correspondence: xiao.xu@uclouvain.be (X.X.); patricia.luis@uclouvain.be (P.L.)

Abstract: Metal–organic frameworks (MOFs), a sub-group of porous crystalline materials, have been receiving increasing attention for gas separation and pervaporation because of their high thermal and chemical stability, narrow window sizes, as well as tuneable structural, physical, and chemical properties. In this review, we comprehensively discuss developments in the formation of continuous MOF membranes for gas separation and pervaporation. Additionally, the application performance of continuous MOF membranes in gas separation and pervaporation are analysed. Lastly, some perspectives for the future application of continuous MOF membranes for gas separation and pervaporation are given.

Keywords: metal–organic frameworks; continuous MOF membranes; formation developments; gas separation; pervaporation



Citation: Xu, X.; Hartanto, Y.; Zheng, J.; Luis, P. Recent Advances in Continuous MOF Membranes for Gas Separation and Pervaporation. *Membranes* **2022**, *12*, 1205. <https://doi.org/10.3390/membranes12121205>

Academic Editor: Liang Ge

Received: 31 October 2022

Accepted: 25 November 2022

Published: 29 November 2022

Publisher's Note: MDPI stays neutral with regard to jurisdictional claims in published maps and institutional affiliations.



Copyright: © 2022 by the authors. Licensee MDPI, Basel, Switzerland. This article is an open access article distributed under the terms and conditions of the Creative Commons Attribution (CC BY) license (<https://creativecommons.org/licenses/by/4.0/>).

1. Introduction

The demand for sustainable and energy-efficient separation and purification technology is growing in order to achieve carbon neutrality. Compared with other traditional separation processes (including amine adsorption, pressure swing adsorption, and cryogenic separation), membrane separation has gained increasing attention from different realms, namely from energy, water, chemical, healthcare, and food areas, because it has unique merits, such as energy efficiency, high separation efficiency, small carbon footprint, low cost, easy operation, and scalability, etc. [1–3]. Among a variety of membranes, semi-permeable membranes are central in gas separation and pervaporation to separate or remove angstrom-scale gas or liquid molecules [4]. Gas separation is considered as one of the most promising technologies to perform continuous, reagent-free, and non-hazardous separation of gases or to obtain mixtures enriched in one component [5,6]. Pervaporation is also an important membrane technology that is typically used to separate minor components from heat-sensitive, close-boiling, and azeotropic mixtures. Compared to traditional distillation, pervaporation is a benign process with high efficiency [7].

Metal–organic frameworks (MOFs) have gained more attention for gas separation and pervaporation because MOFs are a class of porous materials with unique traits, including large surface areas, uniformly adjustable sized pores, high void volumes, and hybrid organic–metal nature [8–12]. Membranes based on these kinds of materials generally have an asymmetric structure with a selective layer positioned on inorganic supports [13]. Up to now, gas separation and pervaporation using continuous MOF membranes are mainly achieved by exploiting the solution–diffusion mechanism of the MOF. Specifically, the solution–diffusion mechanism can be classified into two separation mechanisms: solubility-based separation and diffusivity-based separation [14].

Although there have been several excellent review articles on the application of MOF membranes for gas separation and pervaporation [8,9,15], only continuous MOF membranes applied in gas separation or pervaporation have been summarized. In this work, recent developments, including the fabrications and applications, of continuous MOF membranes for gas separation or pervaporation are systematically summarized and analysed. Moreover, the application performance of continuous MOF membranes for gas separation and pervaporation are evaluated and analysed, respectively. In addition, the major challenges and future perspectives of continuous MOF membranes for gas separation and pervaporation are presented.

2. Developments of the MOF-Based Membrane

As a type of porous material, metal–organic frameworks (MOFs), because of large surface areas, good stability and well-defined pore structures with molecule-scale pore size, show great potential for energy-efficient separations of gas or liquid mixtures [16,17]. Because most MOFs are in the form of either microcrystalline powders or submillimetre crystals, it is difficult to use them widely in the field of separation. To improve the situation, a variety of MOF-based membranes have been prepared. These membranes can in general be classified into two types: continuous MOF-based membranes and MOF-based mixed matrix membranes. In this review, only continuous MOF-membranes are discussed.

2.1. Continuous MOF-Based Membranes

Continuous MOF-based membranes are a class of continuously grown membranes which are mainly prepared by growing uninterrupted polycrystalline or epitaxial layers on substrates. The substrates to support selective MOF layers are typically inorganic. Some efforts have been made to deposit MOF layers on organic substrates over these years [18,19]. In this type of membrane, continuous MOF layers have selectivity to different feed components because the pores of MOFs are the only permeation channel through all layers, while substrates as a support offer mechanical strength for the MOF layers. Since the first attempt to make continuous MOF membranes was reported by Fischer et al. in 2005 [20], there has already been a variety of approaches developed to fabricate continuous MOF films, including in situ growth [21–23], secondary growth [24–26], interfacial diffusion [27–31], liquid phase epitaxy [32–35], vapor deposition [36–41], and the electrodeposition method [42–44].

2.1.1. In Situ Growth

In situ growth is to fabricate continuous MOF-based membranes on substrates by soaking the substrate in solutions of inorganic precursors/organic precursors, as illustrated by Figure 1. The whole process is mainly divided into two steps: the first step is to induce MOF crystal nucleation on the substrate surface under certain conditions, and the second step is to promote the continuous growth of the MOF crystals until the substrate surface is completely covered with a continuous MOF layer [45].

However, it is difficult to achieve sufficient density of nucleation sites on unmodified substrates. To solve this difficulty and at the same time strengthen the adhesion MOF layers and substrates, the supporting substrates are modified. A modification of the substrate surface is sometimes crucial to form crack-free MOF membranes. In summary, in situ growth can be further classified into two routes: in situ growth on an unmodified support and in situ growth on a modified support [9]. Despite many attempts, the fabrication of a defect-free MOF layer on an unmodified substrate remains a challenge. To obtain a defect-free continuous MOF layer while enhancing the adhesion of the MOF layer and the substrate, the substrate usually needs to be modified.

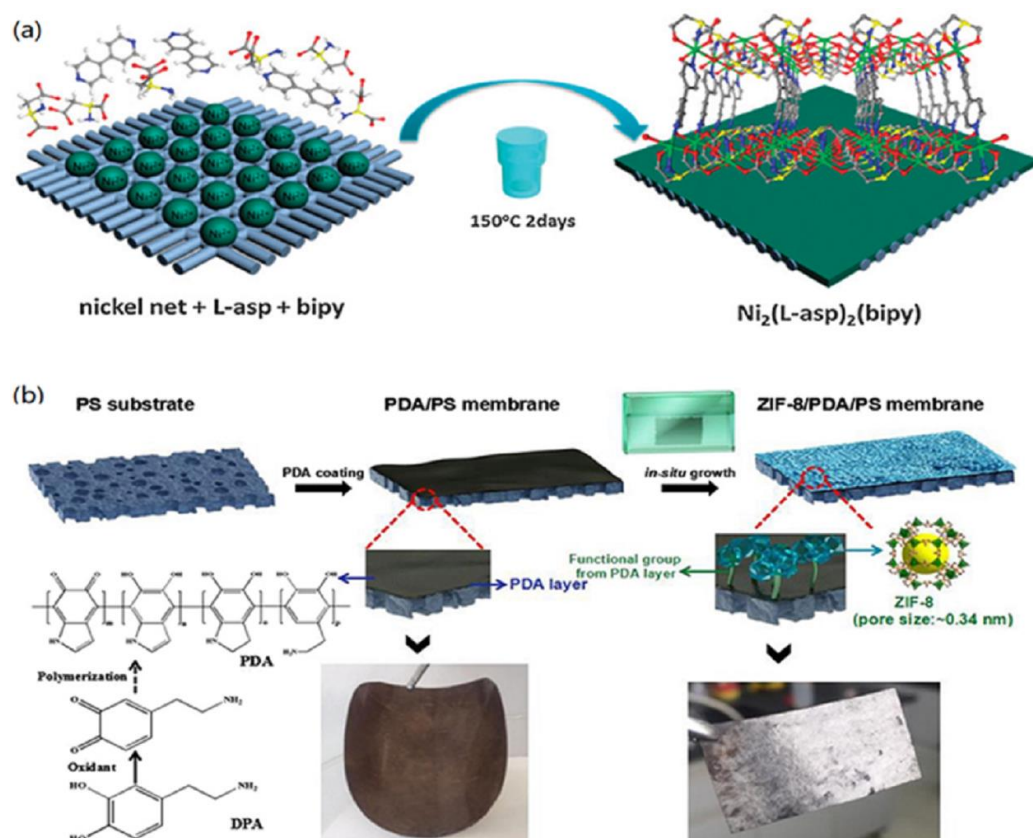


Figure 1. Schematic illustrations of the in-situ synthesis of continuous MOF membranes: (a) the growth of $\text{Ni}_2(\text{L-asp})_2(\text{bipy})$ on an unmodified nickel support and (b) the growth of ZIF-8 membrane on a modified PS support. Reprinted with permission from Refs. [12,40].

As the name suggests, in situ growth of the MOF on an unmodified support is to grow a MOF layer on an unmodified support. The first example of a continuous and well-intergrown MOF-5 membrane was demonstrated by Lai and co-workers [46]. A porous alumina disc was soaked into the mother solution of MOF-5, and then the solution was heated to 105 °C under sealed conditions to prepare continuous MOF-5 membranes. The tested results showed that the diffusion of H_2 , CH_4 , N_2 , CO_2 , and SF_6 through the MOF-5 membrane followed the Knudsen diffusion behaviour. It was reported by Jürgen et al. that by replacing dimethylformamide (DMF) as the solvent and aqueous methanol with absolute methanol, a crack-free, dense and polycrystalline ZIF-8 layer was synthesized on a titania support using an in-situ microwave-assisted solvothermal method [47]. The as-synthesized MOF membrane showed a fine balance between permeance and selectivity for the separation of H_2/CH_4 . To enhance the adhesion between the MOF layer and the substrate, Chen and Wang et al. demonstrated the in-situ growth of ZIF-8 layers on tubular substrates using a concentrated synthesis gel, with a molar composition of Zn, 2-methylimidazole (Hmim), and methanol of 1:8:700, by dip or slip casting [48]. The hollow substrates were first dried at 80 °C overnight and then being placed vertically in an autoclave. Subsequently, the ZIF-8 synthesis solution was slowly poured into the autoclave and heated under the given conditions. The crystalline ZIF-8 layers on the substrates were compact and continuous with a thickness of 6 μm . The EDX elemental mapping suggested that some ZIF-8 crystal might exist in the pores of the supports. The prepared ZIF-8 exhibited strong CO_2 adsorption properties. For the enhancement of Interfacial adhesion, Kang and co-workers used 'single metal source' to generate a homochiral MOF membrane [49]. In this report, the substrate not only played the role of supporting the MOF layer but was also involved in the MOF growth process as the sole nickel source. The

obtained thin and crack-free $\text{Ni}_2(\text{L-asp})_2(\text{bipy})$ exhibited a comparable ee value of 32.5% for the pervaporation separation of pure racemic mixtures.

As noted above, how to enhance the interfacial adhesion is an urgent problem for the preparation of continuous MOF membranes; the modification of the substrate has been considered as an effective strategy to solve this problem. The substrate surface can be modified physically or chemically. Zhang et al. first reported the growth of low-defect ZIF-8 membranes on tubular α -alumina substrates that were modified by coating a layer of ZnO, and then 2-methylimidazole was used to activate and react with the ZnO layers [50]. The resulting ZIF-8 layers on physically modified supports exhibited excellent separation performance. These ZnO layers have an important role in promoting the synthesis of the ZIF-8 membranes because ZnO can be utilized as the secondary metal source for the preparation of MOF membranes. The obtained low-defect membrane exhibited higher permeances for small gas molecules of H_2 , N_2 , and CH_4 , while large molecules of C_3H_8 , $n\text{-C}_4\text{H}_{10}$, and SF_6 had significantly low permeability through the ZIF-8 membranes. For the preparation of defect-free MOF membranes, Tan and co-workers prepared thin uniform ZIF layers on physically modified supports [51]. First, they covered the surface of polypropylene (PP) supports with the metal-chelating polyaniline (PANI) layers by an in situ deposition technique. Subsequently, ZIF-7 and ZIF-67 membranes with controllable thicknesses were produced on the PP supports. The ZIF-7- NH_2 membrane with gate-opening and flexibility showed H_2 permeance of $4.9 \times 10^{-6} \text{ mol m}^{-2} \text{ s}^{-1} \text{ Pa}^{-1}$ and an ideal H_2/CO_2 separation factor of 10.6. Using the physically modified concept, Wu et al. deposited 50–200 nm thick polydopamine (PDA) layers on the $\alpha\text{-Al}_2\text{O}_3$ disks before the in situ solvothermal synthesis of MIL-160 membranes [52]. The obtained high-crystallinity MIL-160 membrane showed the high flux of $467 \text{ g m}^{-2} \text{ h}^{-1}$ and the selectivity of 38.5 from the pervaporation separation of p-xylene from its bulkier isomer o-xylene. Another example of the preparation of HKUST-1 membrane on the chemically modified support via the ‘twin copper source’ technique was reported by Guo and co-workers [53]. In their report, the copper net as both copper source and support for the continuous MOF membrane first went through a series of treatments to reach oxidation, and then the HKUST-1 membrane was synthesized on the oxidised support that was placed vertically in an autoclave full of a solution of HKUST-1. The resulting membrane demonstrated higher permeation flux of H_2 ($\sim 1 \times 10^{-1} \text{ mol} \cdot \text{m}^{-2} \cdot \text{s}^{-1}$) than other gas components in the separation of H_2/CO_2 , H_2/N_2 , and H_2/CH_4 mixtures.

2.1.2. Secondary Growth

Secondary growth (also called seeded-secondary growth) of MOF membranes involves the seeding of a crystal nucleus on the support, followed by the growth of MOF membranes on the seeded support, as illustrated in Figure 2. For the fabrication of MOF membranes, secondary growth has been proved to be more likely to obtain thinner and less defective MOF membranes [54]. Although the crystal nucleation and growth steps of secondary growth can be independently controlled, the control of the final thickness and orientation of MOF membranes can be achieved by controlling the thickness and orientation of the seeded layer [55]. The key step for the secondary growth of MOF membranes is the seeding. Up to now, a variety of seeding techniques has been developed including rubbing [56], dip-coating and slip-coating [57], electro-spinning [58], microwave radiation [59], spin coating [60], reactive seeding [61], and thermal seeding [62], which can be classified into physical seeding and chemical seeding.

In 2009, Tsapatsis et al. synthesized the microporous MOF membrane by manual assembly using a seeded solvothermal growth on an α -alumina support coated with polyethyleneimine (PEI) [63]. In this method, the seeded support was vertically placed in the autoclave containing a mother solution of microporous MOF membrane at 150°C for 12 h, producing an oriented membrane with the pores aligned preferentially perpendicular to the support surface. Such MOF membranes exhibited low H_2 permeances with ideal selectivity for H_2/N_2 of 23. Lai and co-workers also reported on the preparation of a con-

tinuous ZIF-8 membrane [64]. The seeds were first attached on a hollow yttria-stabilized zirconia (YSZ) fibre support by dip-coating and drying, and then the seed support was placed vertically in a glass vial filled with a secondary solution. Subsequently, the glass vial was heated under certain conditions, finally producing a continuous ZIF membrane with a thickness of about 2 μm . In single-component permeation studies, the membrane exhibited a superior performance with H_2 permeance of $\sim 15 \times 10^{-7} \text{ mol/m}^2 \text{ s Pa}$ and an ideal selectivity of $\text{H}_2/\text{C}_3\text{H}_8$ of more than 1000 at room temperature. Wang et al. used a wet-rubbing method to coat $\text{Ni}_2(\text{l-asp})_2\text{bipy}$ crystals on the top surfaces of SiO_2 discs [65]. After this operation, a solvothermal reaction was carried out to prepared continuous grown $\text{Ni}_2(\text{l-asp})_2\text{bipy}$ membrane. To apply this membrane for the pervaporation separation of ethanol from ethanol/water mixture, a PDMS layer was subsequently coated on a $\text{Ni}_2(\text{l-asp})_2\text{bipy}$ layer to switch the wettability of the MOF membrane to the hydrophobicity. The prepared membrane was used to separate the water/ethanol mixture with 50 wt% ethanol at 30 $^\circ\text{C}$, exhibiting a remarkably high flux of $27.6 \text{ kg}\cdot\text{m}^{-2} \text{ h}^{-1}$ and a separation factor of 73.6. For high reproducibility, Jürgen Caro's group used an automatic dip-coating device to attach ZIF-8 seeds on $\alpha\text{-Al}_2\text{O}_3$ supports before the secondary growth in solvothermal conditions [66]. Supported polycrystalline ZIF-8 membranes still did not display a clear cut-off in the pervaporation separation of n-hexane, benzene, and mesitylene.

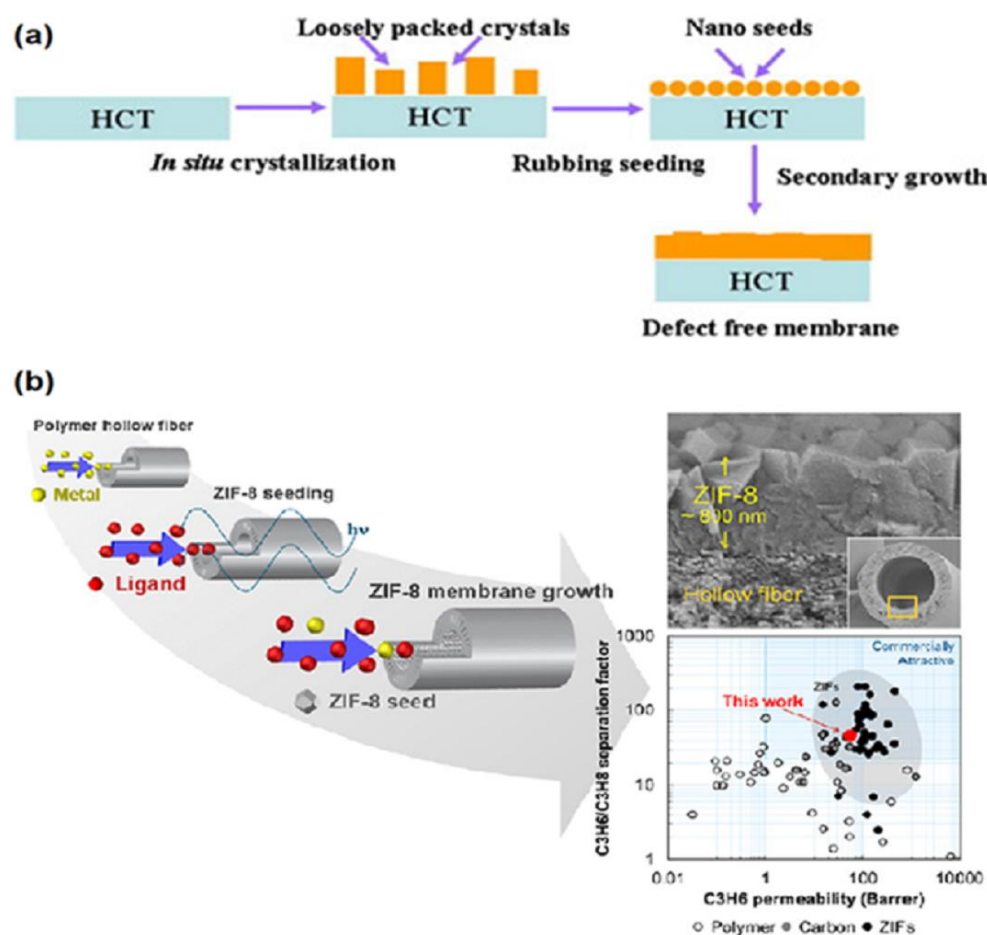


Figure 2. Schematic representations of the secondary growth of MOF membranes: (a) physical seeding and (b) chemical seeding. Reprinted with permissions from Refs. [67,68].

In addition to physical seeding, chemical seeding has been gradually introduced to deposit MOF crystals on the porous substrates. “Thermal seeding” was first reported to anchor MOF seeds on porous substrates by Jeong et al. [62]. In this research, the solution containing HKUST-1 crystals and unreacted HKUST-1 precursors was dropped on hot porous α -alumina supports, and this process repeated until the support surface was covered

sufficiently with seed crystals. The resulting seeded support was placed in the autoclave, into which the solution containing HKUST-1 precursors was then filled. Under appropriate synthesis conditions, a continuous HKUST-1 membrane without cracks and fractures grew on the chemically seeded support. The prepared HKUST-1 membrane showed moderate ideal selectivity of H₂ over N₂, CH₄, and CO₂ for the gas separation, also exhibiting greater affinity to CO₂ over CH₄ and N₂ with the temperature. Another chemical seeding method is facile reactive seeding (RS) [61]. In this method, a porous substrate played dual roles, one as the support to hold the selective layer, and the other as the inorganic source to engage in the growth of MIL-53 seeds on the support. The as-synthesized MIL-53 membrane displayed a sharp separation for the pervaporation separation of H₂O from ethanol, t-butanol, and ethyl acetate, respectively. At 60 °C, when a H₂O-ethyl acetate solution (7 wt.% H₂O) passes through the MIL-53 membrane, the H₂O concentration in the permeate increased to 99 wt.% with the flux of 454 g·m⁻² h⁻¹.

Lee et al. used a combination of microwave-assisted seeding and microfluidic secondary growth to fabricate well-intergrown ultrathin ZIF-8 membranes with a thickness of ~800 nm deposited on porous Matrimid[®] polymer hollow fibres, which was the first time that the ZIF-8 membranes via secondary growth were grown on the bore side of polymeric hollow fibres [68]. They tested binary gas separation performance of the membranes using propylene/propane, showing a separation factor of about 46 and propylene permeance of ~55 GPU (gas permeation unit, 1 GPU = 3.348 × 10⁻¹⁰ mol m⁻² s⁻¹ Pa⁻¹). Using a covalent-assisted seeding method, well-intergrown ZIF-8 membranes were prepared on polyimide substrate [69]. For the successful fabrication of a MOF layer on the polymeric substrate, the imidazole-2-carbaldehyde (ICA) molecules as the covalent agent were first grafted onto the polyimide substrate cross-linked with ethylenediamine (EDA), which offered the reaction sites for anchoring ZIF-8 seeds on polyimide substrate. By this method, a well-grown ZIF-8 layer was firmly coated on the polyimide substrate. The prepared ZIF-8 membrane showed a further elevated separation factor compared to polyimide membrane for the pervaporation dehydration of isopropanol at 40 °C.

2.1.3. Interfacial Synthesis

So far, various methods of interface synthesis have been developed and used successfully in the facile manufacture of MOF membranes. According to the fluid properties of the precursor solution, interface synthesis can be divided into static and dynamic interface synthesis methods (Figure 3) [70].

Static Interfacial Synthesis

Static interfacial synthesis used for obtaining continuous MOF layers can be classified into the following two routes: (1) interfacial diffusion synthesis [71], (2) contra-diffusion synthesis (counter-diffusion synthesis), as shown in Figure 3a,b [72]. In the interfacial diffusion synthesis, two precursors (e.g., the metal ion and the organic ligand) are usually separately dissolved in two immiscible solvents. When two precursor molecules independently meet at the interface in two incompatible solvents, the crystallization that only occurs at the liquid/liquid or liquid/solid interface leads to the formation of the MOF membrane. Similarly, contra-diffusion synthesis has two precursor solutions as well. It differs from the former route in that the two precursor solutions in contra-diffusion synthesis are separated by a porous substrate; two precursor molecules diffuse in opposite directions through the porous channels of the substrate.

Zhu et al. used the interfacial diffusion method to synthesize free-standing continuous MOF membranes [73]. To grow the MOF membrane, the reactant concentration region needed to be identified because a MOF layer was only able to be prepared in the region of high molar ratio of Zn(NO₃)₂ to terephthalic acid (H₂BDC) and low triethylamine (TEA) concentrations, in which TEA was utilized as a catalyst to improve the coordination reaction between Zn(NO₃)₂ and H₂BDC. The resulting membranes were found to be asymmetric including three layers by SEM and XRD, the composition of the surface layer was 3D

$\text{Zn}_4\text{O}(\text{BDC})_3$ (MOF-5) with a particulate morphology, the bottom layer had a sheet-like morphology, and its component was 2D $\text{ZnBDC}\cdot\text{DMF}$ (MOF-2), and in between were transitional zinc-carboxylate structures, viz. $\text{Zn}_3(\text{OH})_2(\text{BDC})_2$ (MOF-69c) and $\text{Zn}_5(\text{OH})_4(\text{BDC})_3$. Due to poor mechanical stability, free-standing continuous MOF membranes have not been widely used in gas separation and pervaporation [9]. Chen et al. prepared a ZIF-8 membrane on porous $\alpha\text{-Al}_2\text{O}_3$ disks via interfacial synthesis [74]. In this method, the pre-treated $\alpha\text{-Al}_2\text{O}_3$ disk was soaking into inorganic precursor solution in an Erlenmeyer flask. To fully fill the pores of the disk with zinc nitrate, the flask was connected to a vacuum. After 30 min, the disk was taken out, and then the excess solution on the disk surface was wiped out using a rubber wiper. Subsequently, the disk was gently soaked into the pre-heated organic precursor solution for the desired time to prepare the ZIF-8 membrane. The obtained ZIF-8 membrane exhibited a CO_2/N_2 separation factor of 5.49 and CO_2 permeance of $0.47 \times 10^{-7} \text{ mol}\cdot\text{m}^{-2}\cdot\text{s}^{-1}\cdot\text{Pa}^{-1}$ in single-gas permeation experiments of CO_2 and N_2 .

Like interfacial diffusion synthesis, the contra-diffusion method has been developed to construct ultrathin MOF membranes. Wang and co-workers successfully prepared ZIF-8 films on flat nylon substrates with the contra-diffusion synthesis method in 2011 [72]. In their research, the zinc nitrate methanol solution and 2-methylimidazole (Hmim) methanol solution were separated by the porous nylon membrane with a pore size of $0.1 \mu\text{m}$. After a certain period of crystallization, the ZIF-8 films were prepared under ambient temperature and deployed to separate the H_2/N_2 gas mixture. The gas permeation results of a H_2/N_2 ideal selectivity of 4.3 with H_2 permeance of $1.97 \times 10^{-6} \text{ mol m}^{-2} \text{ s}^{-1} \text{ Pa}^{-1}$ and N_2 permeance of $0.46 \times 10^{-6} \text{ mol m}^{-2} \text{ s}^{-1} \text{ Pa}^{-1}$ confirmed that the ZIF-8 layers were continuous and compact. In 2013, the same group extended the contra-diffusion synthesis method to synthesize continuous and compact ZIF-8 layers on nylon membranes by using an aqueous solution with a $\text{Zn}^{2+}:\text{Hmim}$ stoichiometric ratio of 1:2 [75]. A $2.5 \mu\text{m}$ thick ZIF-8 layer was formed on the hmim side, exhibiting a H_2/N_2 ideal selectivity of 4.6 in the gas permeation tests.

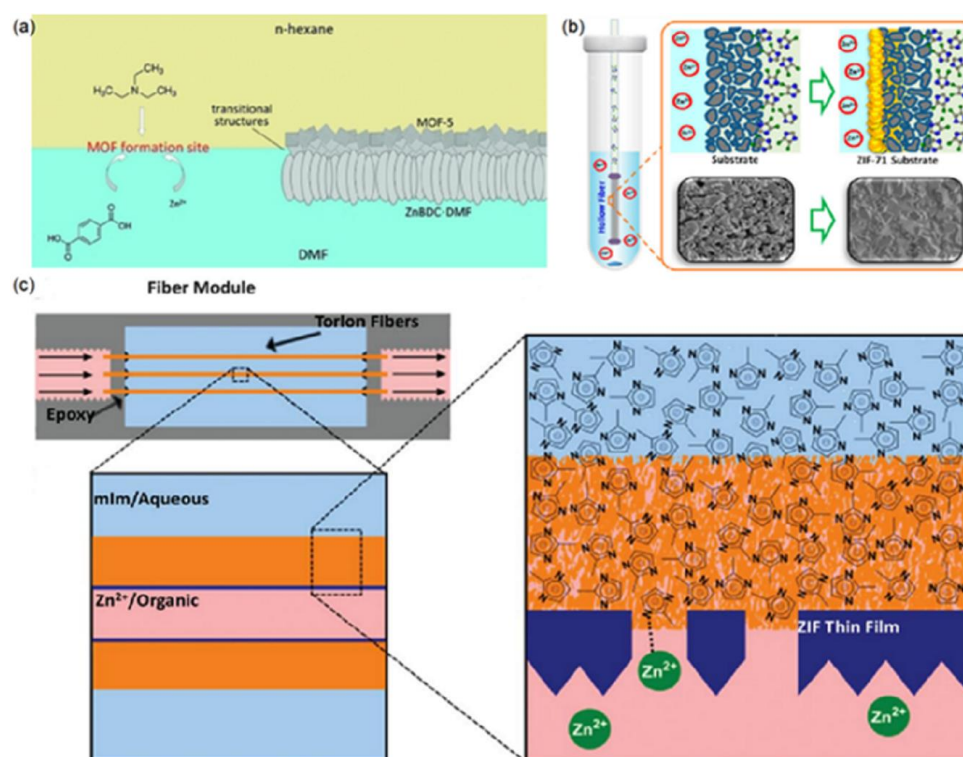


Figure 3. Schematic representations of the interfacial synthesis of MOF membranes (a) interfacial diffusion synthesis [64], (b) contra-diffusion and (c) dynamic interfacial synthesis. Reprinted with permissions with Refs. [73,76,77].

In the contra-diffusion reaction, the substrates used as porous supports were usually commercial microfiltration membranes with large pores (pore diameter > 100 nm) and long channels (over tens of microns). In these cases, the diffusions of metal ions and organic ligands inside these membranes were quite fast and difficult to control, which resulted in the formation of MOF films with defects and/or relatively thick layers [60,78–80]. Considering such problems, a method of fabricating ultra-thin and continuous MOF membranes, a spatially confined contra-diffusion synthesis process, was reported by Zhang and co-workers [80]. In this process, the difference from the previously reported contra-diffusion processes was that an ultra-thin nano-porous membrane made of polydopamine-coated single-wall carbon nanotube (PD/SWCNT) network with small pores or channels of 5–10 nm was deployed as the porous substrate at the liquid–liquid interface instead of commercial microfiltration membranes. By a spatially confined contra-diffusion process, an ultra-thin continuous ZIF-8 film with a thickness of about 550 nm was formed. When applied to hydrogen separation, the membrane showed a high H₂ permeance of up to $6.31 \times 10^{-7} \text{ mol}\cdot\text{m}^{-2}\cdot\text{s}^{-1}\cdot\text{Pa}^{-1}$, while maintaining a high ideal selectivity of 43 for H₂/CO₂. The contra-diffusion method was also utilized to fabricate a ZIF-71 membrane for the pervaporation recovery of ethanol from H₂O [76]. At 25 °C, the synthesized ZIF-71 hollow fibre membrane displayed a comparable performance with a flux of 2.601 g/m² h and a separation factor of 6.88.

Dynamic Interfacial Synthesis

Dynamic interfacial synthesis mainly refers to interfacial microfluidic membrane processing (IMMP). Prior to IMMP, microfluidic processing was deployed to grow continuous MOF membranes on the substrates by flowing mixed precursors in the hollow fibre. Huang and co-workers successfully deposited the ZIF-8 film with a thickness of 2.0 µm on the inner surface of a ceramic hollow fibre by microfluidic processing [81]. The as-synthesized ZIF-8 film on the inner-side of the ceramic hollow fibre was used to recover H₂, displaying good performance with a H₂ permeance of $4.324 \times 10^{-7} \text{ mol}^{-2}\text{s}^{-1}\text{Pa}^{-1}$ and H₂/CH₄ ideal selectivity of 12.13. Using a similar method, the ZIF-93 membrane [82] and the defect-free ZIF-8 membrane [68] were fabricated on the inner surface of the co-polyimide P84 hollow fibre and the Matrimid hollow fibre, respectively. To avoid the occurrence of bulk MOF crystallization during microfluidic processing, Nair and Jones et al., combining microfluidic processing and interface synthesis, proposed interfacial microfluidic membrane processing (IMMP) for the production of ZIF-8 membranes on torlon hollow fibres [77]. Distinguished from the microfluidic synthesis with mixed precursor solution, a Zn²⁺/1-octanol solution was passed through the bore of the hollow fibre, while a 2-methylimidazole (2-mIm)/H₂O solution maintained stationary on the shell side. A continuous and thin ZIF-8 membrane was synthesized on the inner surface of the hollow fibre, due to the relatively fast diffusion of reactants to the water-oil interface under continuous flow. By contrast, under static growth conditions, dense and noncontinuous layers of ZIF-8 particles were produced owing to the insufficient supply of Zn²⁺ ions to maintain the growth of the film after the initial nucleation and growth of ZIF-8 crystals on the inner surface of the fibre. The prepared ZIF-8 membranes with a thickness of 9 µm were used to distinguish H₂ from C₃H₈ and C₃H₆, exhibiting moderate and efficient selectivity. From the above example, we can conclude that the so-called IMMP involves the combination of membrane module construction and the crystallization mechanism of interface diffusion synthesis or contra-diffusion synthesis. The two non-mixed precursors flow on the tube and shell sides of the hollow fibre respectively. The MOF film is deposited on the surface of the hollow fibre by the flowing precursors. Employing the same concept, Marti et al. synthesized continuous defect-free ZIF-8 thin films on the outer surface of polymeric hollow fibre using continuous precursor flow, in which a Zn²⁺/H₂O solution was flowed on the shell side of hollow fibre, and at the same time 2-methylimidazole (MeIm)/H₂O was passed through the bore of the hollow fibre [83]. The prepared ZIF-8 membrane was applied to capture CO₂, demonstrating a CO₂ permeability of 22 GPU and a highest reported CO₂/N₂ selectivity of 52.

2.1.4. Liquid Phase Epitaxy (LPE)

For liquid-phase epitaxy (LPE, also known as layer-by-layer) growth, also referred to as stepwise layer-by-layer (LBL) assembly, a substrate is exposed to one type of MOF precursor component (typically two types) at a time, and repeatedly cycled between organic secondary building units (SBUs) and inorganic SBUs by manual immersion [84], dipping [85], spraying [86], or spin coating [87]. Unreacted components are usually removed by rinsing a solvent between successive deposition steps, as illustrated in Figure 4. The orientation and the thickness of the MOF membrane in the vertical direction to the substrate (out-of-plane) can be precisely controlled by LPE. Moreover, the sequential and stepwise method gives each kind of precursor component the opportunity to saturate all the possible deposition sites without forming new nucleus on the surface or in the solution, thereby forming a low-defect membrane. The layer-by-layer growth mode for the fabrication of MOF membranes can be traced to the pioneering work of Wöll and co-workers [88]. They grew a MOF layer on COOH-terminated self-assembly monolayers (SAM) using a layer-by-layer approach in which SAM was repeatedly manually immersed in a solution of metal precursor and in the organic precursor solution. While there is no doubt that the manual immersion technique used in LPE applications can result in smoother MOF membranes, called surfaced-attached MOFs (SURMOFs), there is one major drawback: it is not efficient to prepare SURMOF membranes. Some improved strategies, based on the manual liquid-phase epitaxy synthesis route, are emerging to design SURMOF membranes on the substrate. For example, an automated, computer-controlled dipping robot has been deployed for the preparation of SURMOF membranes of ZIF-8 on Au-coated α -Al₂O₃ supports by Valadez Sánchez and co-workers [89]. The obtained ZIF-8 SURMOF membranes exhibited higher hydrogen and ethene permeances due to their smaller molecular sizes.

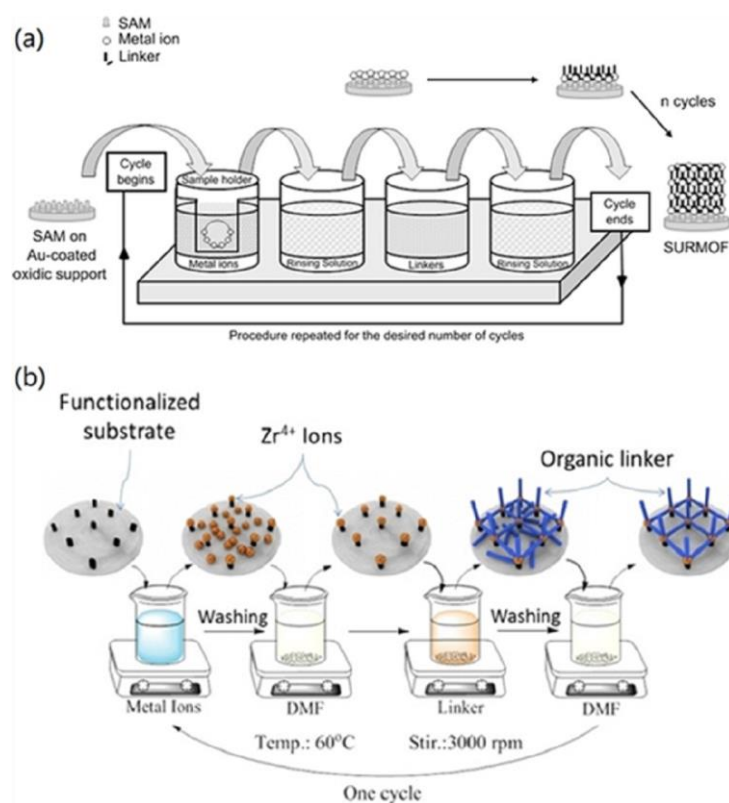


Figure 4. Schematic diagrams for the LPE growth of MOF membranes: (a) ZIF-8 SURMOF membrane deposited on a Au coated alumina support and (b) UiO-66-NH₂ SURMOF membrane deposited on a flat gold-coated substrate. Reprinted with permissions from Refs. [89,90].

In 2014, Eddaoudi and co-workers reported the assembly of ultra-thin and defect-free ZIF-8 selective layers on porous aluminate supports by precisely controlling the epitaxial growth [85]. In the single-gas permeation tests of He, H₂, CO₂, O₂, N₂, CH₄, C₂H₄, C₂H₆, C₃H₆, C₃H₈, and n-C₄H₁₀, the resultant ZIF-8 membranes were observed to have a cut-off for the diffusion coefficient between C₂ and C₃ because of the relatively small window size of ZIF-8. Although the ZIF-8 membranes fabricated by LPE exhibited about 100 times lower permeance but with good ideal selectivity of 5, 11, 12, and 60 for H₂-CO₂, H₂-N₂, H₂-CH₄, and H₂-C₃H₈, respectively, at 308 K, suggesting the synthesized ZIF-8 membranes with minimal grain boundary micro-defects.

Recently, the Léon group used the LPE method and an in situ growth method to prepare an UiO-66-NH₂ SURMOF membrane and an UiO-66-NH₂ membrane, respectively [91]. In the equimolar case, the UiO-66-NH₂ SURMOF membrane exhibited a higher H₂/N₂ separation factor of 3.02 because of the LPE method continuously generating a highly oriented MOF membrane.

2.1.5. Vapor Deposition

For the MOF membranes by chemical solution deposition (CSD) typically involving reacting metal salts and organic ligands in solutions, the advantages provided are generally simplicity and effectiveness, low capital cost of laboratory implementation, compatibility with conventional wet chemical operations, and high chemical flexibility. However, the reactant transport and fluid dynamic processes of CSD are usually complex and are very difficult to control carefully, especially on an industrial scale. In contrast to CSD, vapor deposition of MOF membranes can facilitate their implementation in lab-scale research and industries. Usually, each vapor deposition process includes three steps: (1) evaporation, (2) the transportation of the vaporized material, (3) deposition of the film on the substrate. As of now, while there are many variations of vapor deposition, the processes can typically be divided into two categories: physical vapor deposition (PVD) and chemical vapor deposition (CVD), as shown in Figure 5a,b [92].

The PVD is a purely physical process in which the target material is evaporated into the gas phase and deposited onto the substrate for the preparation of the thin films without any chemical reaction taking place. The most critical step in the entire process is the initial evaporation of the target material, which can be achieved by various methods, such as conventional thermal evaporation, ion plating, sputtering, or pulsed-laser deposition (PLD). However, it is quite difficult to apply PVD to the fabrication of the MOF due to low vapor pressure and thermal decomposition or amorphization of MOFs from thermal stress, ion bombardment, or laser irradiation [93,94]. To remedy those limitations, the femto-PLD technique was utilized to fabricate porous ZIF-8 membranes for the first time [94]. To prevent its structural degradation and decomposition, polyethylene glycol 400 (PEG-400) was deployed as a “vehicle” to impregnate with ZIF-8, and then hybrid ZIF-8 soaked with PEG-400 was ablated in an ultrahigh vacuum chamber, finally forming membranes with approximate composition Zn(C₃N₂H₂-CH₃)₂·¹/₆PEG-400 through the femto-laser technique. The PEG additive in the membranes could be removed by washing with ethanol. However, MOF membranes prepared by PVD for gas separation and pervaporation have not reported so far.

In contrast to PVD, CVD typically involves a chemical reaction between solid and gas phases. In other words, this deposition method is based on the reaction of vaporized substances with the substrate, with the growing layer and/or with each other to form a uniform layer. Up to now, several different routes have been explored using CVD for the preparation of MOF films, mainly including atomic layer deposition (ALD) and molecular layer deposition (MLD). The ALD is a vapor-phase thin layer deposition method based on alternating surface reactions between two precursor gas pulses. This self-limiting growth mechanism well controls the conformal deposition of the layers with nanometre precision thickness [95]. The MLD is a method similar to ALD. In MLD, a layer of molecules is deposited during one self-limiting surface reaction step instead of the deposition of

monolayer of atoms. In 2013, Salmi and co-workers deposited MOF-5 films from the vapor phase by ALD [96]. In their study, it was found that the as-deposited layers were amorphous and nonporous. For forming porous MOF-5 thin membranes, the as-deposited membranes also required a two-step post-deposition crystallization treatment. In 2018, the smooth, pinhole-free ZIF-8 thin layers were uniformly deposited on porous substrates using ALD [97]. In one ALD cycle, a $\sim 5\text{-}\mu\text{m}$ γ -alumina mesoporous layer with pores in the 2 to 5 nm range was first coated on an α -Alumina macroporous substrate, then diethylzinc was deposited on the γ -alumina mesoporous layer using ALD, and the diethylzinc layer was finally exposed to water vapor to yield hydroxylated zinc oxide. This ALD cycle was repeated for up to 50 times for the preparation of an impermeable zinc oxide layer coated on γ -alumina layer. This impermeable material can be transformed into a porous ZIF-8 membrane by exposure to vapor of 2-methylimidazole. For the separation of propylene/propane, the resultant porous ZIF-8 membrane enabled a propylene/propane selectivity over 100 with a propylene permeance as high as 114 GPU.

Nilsen and co-workers reported that the film of amino-functionalized UIO-66 was deposited through an all-gas-phase ALD/MLD [98]. Both ZrCl_4 and 2-amino-1,4-benzene dicarboxylic acid (2-amino-1,4-BDC) were utilized as precursors to perform the ALD/MLD depositions in an F-120 Sat-type ALD reactor. The as-formed films could be crystallized by post-deposition treatment. In 2020, Lausund et al. reported on MOF thin films with bi-aromatic linkers deposition by MLD [99]. Although some progress for the fabrication of MOF membranes using MLD has been made, there are no reports on the application of MOF membranes prepared via MLD for gas separation and pervaporation because MOF membranes fabricated using this method generally require a postdeposition treatment to convert amorphous MOF layers into crystalline MOF layers [100].

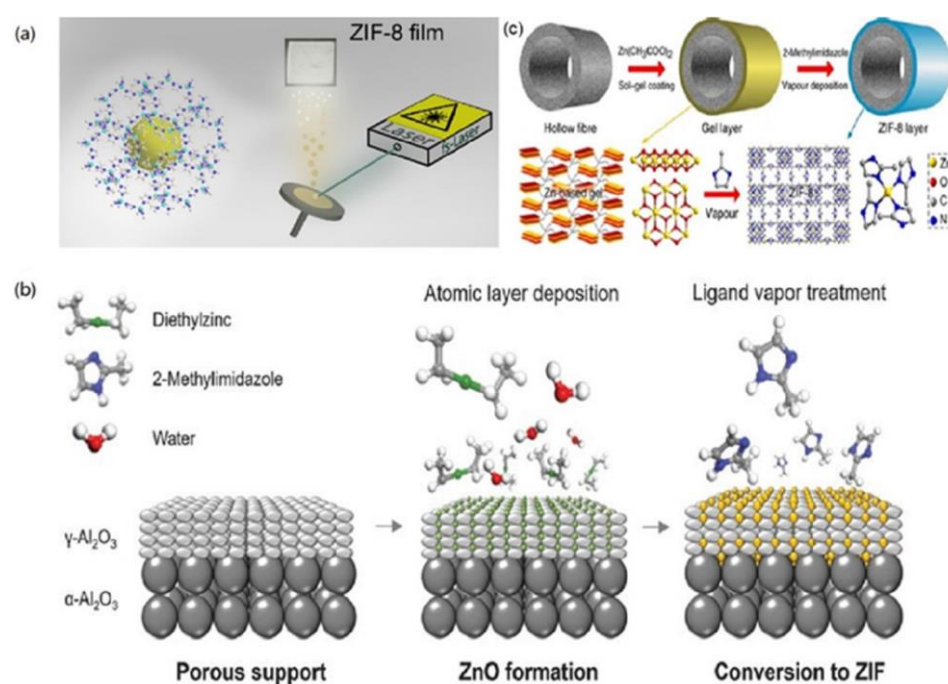


Figure 5. Schematic of MOF membrane formation processes using vapor: (a) ZIF-8 membrane deposition via PVD, (b) ZIF-8 membrane deposition via CVD and (c) ZIF-8 membrane deposition via GVD. Reprinted with permissions from Refs. [94,97,101].

To easily produce the MOF membrane with large effective membrane areas, Li and co-workers developed a gel-vapor deposition (GVD) method for preparing ultrathin ZIF-8 membranes by a combination of modification-free sol-gel coating and solvent-free vapor deposition (Figure 5c) [101]. In this method, the Zn-based gel, composed of zinc acetate dihydrate and ethanolamine, was first coated on ammoniated polyvinylidene fluoride

(PVDF) hollow fibres by heat treatment. Then, the organic groups of the gel were substituted through ligand vapor deposition by heat treatment, forming the ZIF-8 membrane. Due to the smaller kinetic diameter of H_2 , H_2 permeance through the resultant ZIF-8 membrane was up to $215.4 \times 10^{-7} \text{ mol m}^{-2} \text{ s}^{-1} \text{ Pa}^{-1}$ with a H_2/C_3H_8 selectivity of as high as 3400.

2.1.6. Electrodeposition

A major disadvantage of many of the methods described above is that defects are randomly generated during the MOF membrane processing. Although a relatively thick membrane can minimize defects, it inevitably reduces the permeability of the membrane [102]. Moreover, a large amount of waste is produced during the fabrication process, especially given the inorganic salts used and the risks and costs related to anions such as nitrate and chloride ions [103]. Electrochemical deposition stands out among the methods of preparing MOF membranes.

The electrochemical method is advantageous because it requires a relatively minor or non-pretreated substrate, shorter growth time, and milder preparation, and is easier to scale up. More importantly, this method allows for controlling the morphology and thickness by altering the current. In principle, there are three routes for making MOF thin membranes by the electrochemical method, namely anodic dissolution, cathodic deposition, and electrophoretic deposition (Figure 6) [102,104]. Anodic dissolution is based on the dissolution of a metal plate used as the anode and the inorganic source for the formation of MOF membranes, and subsequently the released metal ions react with the organic ligands in the electrolyte [103]. During the cathodic deposition process of MOF membranes, electrodes are utilized as chemically inactive spectators and only serve as a source of electrons. Hydroxide formed from the reduction reaction raises the pH of the electrolyte near the cathode and promotes the nucleation and crystal growth of MOFs on the substrate containing the respective organic and inorganic precursor by deprotonating organic ligands [43]. As for electrophoretic deposition, the charged MOF particles (possibly due to missing linkers or missing metal nodes) result in an electric field formation in the electrolyte, in practice, which drives the charged particles toward the oppositely charged electrode to form a MOF layer [105].

The HKUST-1 membrane was among the first MOF membranes to be electrochemically fabricated by researchers at BASF and is also the first MOF membrane reported that has been deposited on a substrate by anodic dissolution [106,107]. During the process, the solvent was continuously stirred, resulting in the removal of crystals formed from the anode surface, resulting in the continuous production of MOF particles. Since then, MOF layers synthesized on the anode have been used to detect nitro compound explosives [108], glucose [109], and to store charge in the electrical double layer [110], as well as in separation [111,112]. So far, the development of electrochemical MOF deposition on other conductive substrates (including indium tin oxide (ITO), fluorine tin oxide (FTO), and glassy carbon) by anodic dissolution has been far behind that achieved by cathodic deposition [113]. To open up new possibilities for producing MOF layers on transparent conductive substrates, the Oliver group confirmed using a modified scheme that a series of MOF thin layers were deposited on indium tin oxide (ITO) glass by anodic dissolution [114]. Before partial dissolution of the anode and initial nucleation of the MOF crystals, the ITO support needed to be electrocoated with either copper or zinc microcrystalline films (Cu-ITO and Zn-ITO), respectively. These metallic coatings served as the metal cation source to grow HKUST-1 and the two-dimensional (2D) cationic framework $[Cu(C_{10}H_8N_2)^{2+}]Br_2$ (CBBr) on Cu-ITO substrates, and $Zn_6(OH)_3(BTC)_3(H_2O)_3 \cdot 7H_2O$ (Zn-BTC, BTC = benzene tricarboxylate) and the 2D framework $[Zn(BPDC)-(H_2O)] \cdot H_2O$ (Zn-BPDC, BPDC = 2,2'-bipyridine-5,5'-dicarboxylate) on Zn-ITO substrates. In 2009, Ameloot et al. electrochemically deposited a MOF layer on an anodic surface by careful modification of the conditions used to synthesize bulk MOF material [115]. In their report, by applying an appropriate electrical voltage to the anodic electrode, the electrochemical oxidation of Cu-atoms on the anode led to the dissolution of Cu (II) ions, which were subsequently introduced into the electrolyte containing 1,3,5-

benzenetricarboxylic acid (BTC) and methyltributylammonium methyl sulfate (MTBS) as a conduction salt. It was found that densely packed films of $[\text{Cu}_3(\text{BTC})_2]$ crystallites with sizes of 2–50 μm could be easily grown by simple alterations of voltage and the composition of the electrolyte. Up to now, there are not practical applications of MOF membranes prepared by anodic deposition for gas separation and pervaporation.

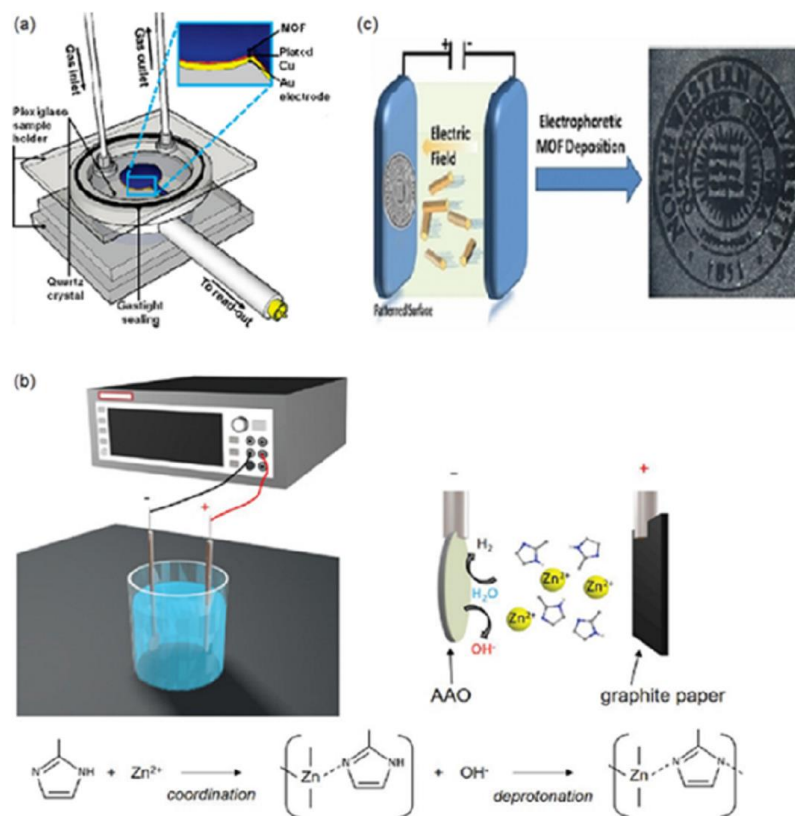


Figure 6. Illustration of electrodeposition of MOF membranes: (a) anodic deposition of $[\text{Cu}_3(\text{BTC})_2]$ membrane, (b) cathodic deposition of ZIF-8 membrane and (c) electrophoretic deposition of MOF membranes. Reprinted with permissions from Refs. [102,105,115].

A disadvantage of anodic dissolution is that the anode is necessarily corroded during the fabricating process of the MOF membrane, which can only apply to a few MOF membranes. To avoid this disadvantage, Dincă et al. illustrated that $\text{Zn}_4\text{O}(\text{BDC})_3$ (MOF-5; BDC = 1,4-benzenedicarboxylate) was deposited at ambient temperature by cathodic electrodeposition [116]. Electrodes were used as chemically inert spectators that did not provide metal ions but provided electrons for the MOF membranes in the cathodic deposition process. To eliminate the potential negative effects on the environment caused by organic solvents, Wei and co-workers developed an aqueously cathodic deposition (ACD) approach to prepare the ZIF-8 membranes, adopting 100% water as the sole solvent instead of a supporting electrolyte or modulator [102]. In the electrolyte cell, anodic aluminium oxide (AAO) with the coating of a conductive layer was deployed as the working electrode, while the counter electrode was graphite paper without any pre-treatment. The two electrodes were parallelly separated by 1.5 cm and soaked in a ZIF-8 precursor solution and zinc cations were driven by electrical field towards the substrate to form a ZIF-8 membrane in only 60 min. The as-formed membrane demonstrated a best combination of 182 GPU permeance and 142 selectivity for the separation of $\text{C}_3\text{H}_6/\text{C}_3\text{H}_8$ mixtures.

Besides anodic dissolution and cathodic deposition methods, the electrophoretic deposition (EPD) method was also used to deposit the MOF membranes [105]. As-synthesized MOFs displaying net negative charges were first suspended in a toluene solution by sonication, and subsequently two identical fluorine-doped tin oxide (FTO) glass substrates as

transparent conductive electrodes were placed in the MOF deposition solution. Partially charged MOF particles were finally driven towards the oppositely charged electrode to form MOF membranes under 90 V. In 2015, Zhu et al. deposited HKUST-1 membranes on porous stainless steel by the EPD method under 100 V for 120 s. In the single gas permeation experiments, the resultant HKUST-1 membrane exhibited the Knudsen separation factors 4.6 for H₂/CO₂, and 3.9 for H₂/N₂ [117].

2.1.7. Other Methods

Recently, some other methods have been developed to fabricate continuous MOF membranes for gas separation and pervaporation. For example, Wang et al. utilized the melting properties of some MOFs including ZIF-62, ZIF-76, and TIF-4, to deposit the molten ZIF-62 phase on porous ceramic aluminate supports [118]. The molecular sieving ability of the as-synthesized ZIF-62 membrane was remarkably enhanced, giving a high separation factor up to 50.7 for H₂/CH₄, 34.5 for CO₂/N₂, and 36.6 for CO₂/CH₄. A new non-conventional approach for the fabrication of a continuous MOF membrane was reported [119]. In this method, a high pressure of 10,000 psi was used to press SIM-1 crystals into a wafer, and then the pressed wafer was treated with ethylenediamine to generate a free-standing SIM-1 membrane. The resulting SIM was used to separate water from water/ethanol mixtures at room temperature in pervaporation, exhibiting a flux of 460 g/m²·h with no ethanol detected in the permeate.

3. Application of Continuous MOF Membranes

3.1. Mechanisms for Gas Separation and Pervaporation

In gas separation and pervaporation, the solution-diffusion mechanism governs transportation permeance and selectivity of molecules across the membrane. Specifically, there are two factors (solubility and diffusivity) that play an important role in gas separation and pervaporation. The solubility of the targeted molecule relies on its interaction with the membrane material while the size of the targeted molecule, with respect to the window and pore sizes of the MOF, determines its diffusivity [14].

The solubility of the gas or liquid molecules is closely related to the equilibration between the gas or liquid molecules and the MOF, and therefore the adsorbent selectivity and adsorption capacity of the MOF play pivotal roles in solubility-based separations [120]. In this case, the membrane material will adsorb preferentially the targeted molecule while the window size of the MOF is larger than the kinetic diameters of all the gas or liquid molecules. If the desorption ability of the targeted molecules downstream is ideal enough to allow for faster diffusion of the targeted molecule, good separation results [14]. However, the solubility of the gas or liquid molecules on the MOF membrane is complicated because there is competition between limited adsorption sites as well as the potentials for cross-adsorbate interactions [120–122]. Recently, Matzger et al. presented a spectroscopic approach to accurately measure the adsorption behaviour in binary gas mixtures that will aid in the initial screening of adsorbents for specific applications [120].

In the diffusivity-based separation, the unique pore structures (window and pore sizes) of MOFs (Table 1) determine the separation performance. In this situation, the window size of the MOF falls between the target molecule and the other molecule. The targeted molecule can pass through the channels provided by the MOF while the other molecule will be blocked outside of the pores of the MOF. Notably, the frameworks of some MOFs are flexible, which will lead to the molecule with a kinetic diameter larger than the window size of the MOF passing through its corresponding membrane. In addition, the nonselective grain boundary effect and the inevitable linker rotation are also unneglectable factors [123].

Table 1. Brief overview of structural parameters of MOFs utilized in gas separation and pervaporation.

MOF Name	Metal	Ligand	Formula Composition	Pore Volume (cm ³ /g)	BET Surface Area (N ₂) (m ² /g)	Window Size (Å)	Ref.
UiO-66	Zr	1,4-benzenedicarboxylate (BDC)	Zr ₆ O ₄ (OH) ₄ (BDC) ₆	0.36	970	6	[124]
MOF-5 (Zn)	Zn	BDC	Zn ₄ O(BDC) ₃	1.4	3800	12	[125]
ZIF-71	Zn	4,5-dichloroimidazole (dcIm)	Zn(dcIm) ₂	0.452	1007	4.8	[126]
CAU-10-H	Al	benzene-1,3-dicarboxylate (1,3-H ₂ BDC)	[Al(OH)(benzene-1,3-dicarboxylate)]·nH ₂ O	0.43	635	7	[127]
ZIF-7	Zn	Benzimidazole (H-bIm)	Zn(bIm) ₂	0.207	380	3	[128]
ZIF-8	Zn	2-Methylimidazole (Hmim)	Zn(mim) ₂	0.554	1344	3.4	[126]
Sm-DOBDC	Sm	2,5-dihydroxy-1,4-benzenedicarboxylate (DOBDC)	Sm ₆ (OH) ₈ (DOBDC) ₆	0.263	520	N/A	[129]
SIM-1(ZIF-94)	Zn	4,5-imidazolecarboxaldehyde	Zn(4-methyl-5-imidazolcarboxaldehyde) ₂	0.19	471	2.6	[130,131]
CAU-1	Al	2-amino-1,4-benzene dicarboxylic acid (H ₂ BDC-NH ₂)	Al ₈ (OH) ₄ (OCH ₃) ₈	0.59	1021.7	4	[132]
MIL-100	In	1,3,5-benzenetricarboxylic acid (H ₃ BTC)	In ₃ O(H ₂ O) ₂ OH(BTC) ₂	0.636	1456	4.6 and 8.2	[133]
ZIF-62	Zn	Imidazole (Im) and benzimidazole (Bim)	Zn(Im) _{1.75} (Bim) _{0.25}	0.20	257	1.4	[134,135]
Ni ₂ (L-asp) ₂ (bipy)	Ni	L-aspartic acid and 4,4'-bipyridine (L-asp and bipy)	Ni ₂ (L-asp) ₂ (bipy)	N/A	247 (CO ₂)	3.8 Å × 4.7 Å	[136]
ZIF-90	Zn	imidazolate-2-carboxyaldehyde (ICA)	Zn(ICA) ₂	0.561	1360	2.86	[126]
UiO-66-NH ₂	Zr	2-amino-1,4-benzenedicarboxylic acid (H ₂ BDC-NH ₂)	Zr ₆ O ₄ (OH) ₄ (BDC-NH ₂) ₆	0.48	1073	7.5	[137,138]
MIL-96	Al	H ₃ BTC	Al ₁₂ O(OH) ₁₈ (H ₂ O) ₃ (Al ₂ (OH) ₄ [BTC] ₆ ·24H ₂ O)	0.24	629.98	3.6 Å × 4.5 Å	[139,140]
HKUST-1	Cu	benzene 1,3,5-tricarboxylate (BTC)	Cu ₃ (BTC) ₂ (H ₂ O) ₃	0.75	1663	9	[141]

3.2. Continuous MOF Membranes in Gas Separation

The intrinsic pore structures of MOFs have resulted in the surge of interest in developing continuous MOF membranes for hydrogen purification, CO₂ removal, and propylene-propane separation. Table 2 summarizes the gas permeation properties of continuous MOF membranes fabricated by different methods. The H₂/CO₂, CO₂/N₂, CO₂/CH₄ and C₃H₆/C₃H₈ separation performance of continuous MOF membranes are drawn against the upper bounds in Figure 7.

Table 2. Continuous MOF membranes for gas separation.

MOF	Support	Method	Permeance (GPU)						Selectivity				Ref.
			H ₂	CO ₂	CH ₄	N ₂	C ₃ H ₆	C ₃ H ₈	H ₂ /CO ₂	CO ₂ /N ₂	CO ₂ /CH ₄	C ₃ H ₆ /C ₃ H ₈	
HKUST-1	N/A	in situ	4716.42	1149.25	1901.49	1402.99	N/A	N/A	4.10	0.82	0.60	N/A	[142]
HKUST-1	PVDF	in situ	6000	1044.78	1761.19	1313.43	N/A	N/A	5.74	0.80	0.59	N/A	[143]
MOF-5	alumina	secondary growth	2388.06	746.27	1164.18	895.52	N/A	N/A	3.20	0.83	0.64	N/A	[59]
ZIF-8	TiO ₂	in situ	179.1	38.81	14.93	14.93	N/A	N/A	4.61	2.60	2.60	N/A	[47]
ZIF-7	alumina	secondary growth	220.9	32.84	35.22	32.84	N/A	N/A	6.73	1.00	0.93	N/A	[144]
ZIF-90	Torlon® fiber	secondary growth	567.16	310.45	208.96	89.55	N/A	N/A	1.83	3.47	1.49	N/A	[145]
ZIF-90	alumina	in situ	626.87	38.81	32.84	35.82	N/A	N/A	16.15	1.08	1.18	N/A	[146]
HKUST-1	Cu net	in situ	379.1	83.58	47.76	83.58	N/A	N/A	4.54	1.00	1.75	N/A	[53]
ZIF-8	alumina	in situ	N/A	N/A	N/A	N/A	24.15	0.59	N/A	N/A	N/A	41.00	[147]
[Ni ₂ (L-asp) ₂ (bipy)]	nickel mesh	secondary growth	3044.78	134.93	385.07	249.85	N/A	N/A	22.57	0.54	0.35	N/A	[148]
ZIF-8	Torlon	interfacial synthesis	1710.8	N/A	N/A	N/A	22.9	2.5	N/A	N/A	N/A	12.00	[77]
ZIF-8	alumina	Electrodeposition	5133	N/A	N/A	N/A	386	3.22	N/A	N/A	N/A	120.00	[149]
ZIF-90	alumina	in situ	850.75	37.61	8	N/A	N/A	N/A	22.62	N/A	4.70	N/A	[150]
ZIF-94	P84®	in situ	12.54	3.5	0.1	N/A	N/A	N/A	3.58	N/A	35.00	N/A	[151]
CAU-1	alumina	secondary growth	1515.5	3940.3	266.24	150.39	N/A	N/A	0.38	26.20	14.80	N/A	[152]
MIL-100	alumina	in situ	N/A	5283.58	4477.61	1462.69	N/A	N/A	N/A	3.61	1.18	N/A	[153]
UiO-66	alumina	Liquid phase epitaxy	313.43	1047.76	35.82	20.9	N/A	N/A	0.30	50.13	29.25	N/A	[154]
ZIF-62	alumina	melt-quenching	56.72	35.82	1.14	1.05	N/A	N/A	1.58	34.11	31.42	N/A	[118]
ZIF-8	alumina	interfacial synthesis	N/A	140.3	N/A	25.56	N/A	N/A	N/A	5.49	N/A	N/A	[74]
ZIF-8	nylon	interfacial synthesis	3373.13	N/A	N/A	746.27	N/A	N/A	N/A	N/A	N/A	N/A	[75]
ZIF-8	torlon	interfacial synthesis	N/A	22	N/A	0.42	N/A	N/A	N/A	52.38	N/A	N/A	[83]
ZIF-8	alumina	liquid-phase epitaxy	56.72	5.97	12.24	5.67	1.79	0.51	9.50	1.05	0.49	3.51	[85]
UiO-66-NH ₂	alumina	liquid-phase epitaxy	35,671.64	N/A	N/A	8268.66	N/A	N/A	N/A	N/A	N/A	N/A	[91]
ZIF-8	alumina	vapor deposition	N/A	N/A	N/A	N/A	479.4	6.48	N/A	N/A	N/A	73.98	[97]
ZIF-8	PVDF	vapor deposition	64,298.51	22,568.35	3592.1	4258.18	2498.94	56.16	2.85	5.30	6.28	44.50	[155]
ZIF-8	alumina	Electrodeposition	N/A	N/A	N/A	N/A	182	1.28	N/A	N/A	N/A	142.19	[102]

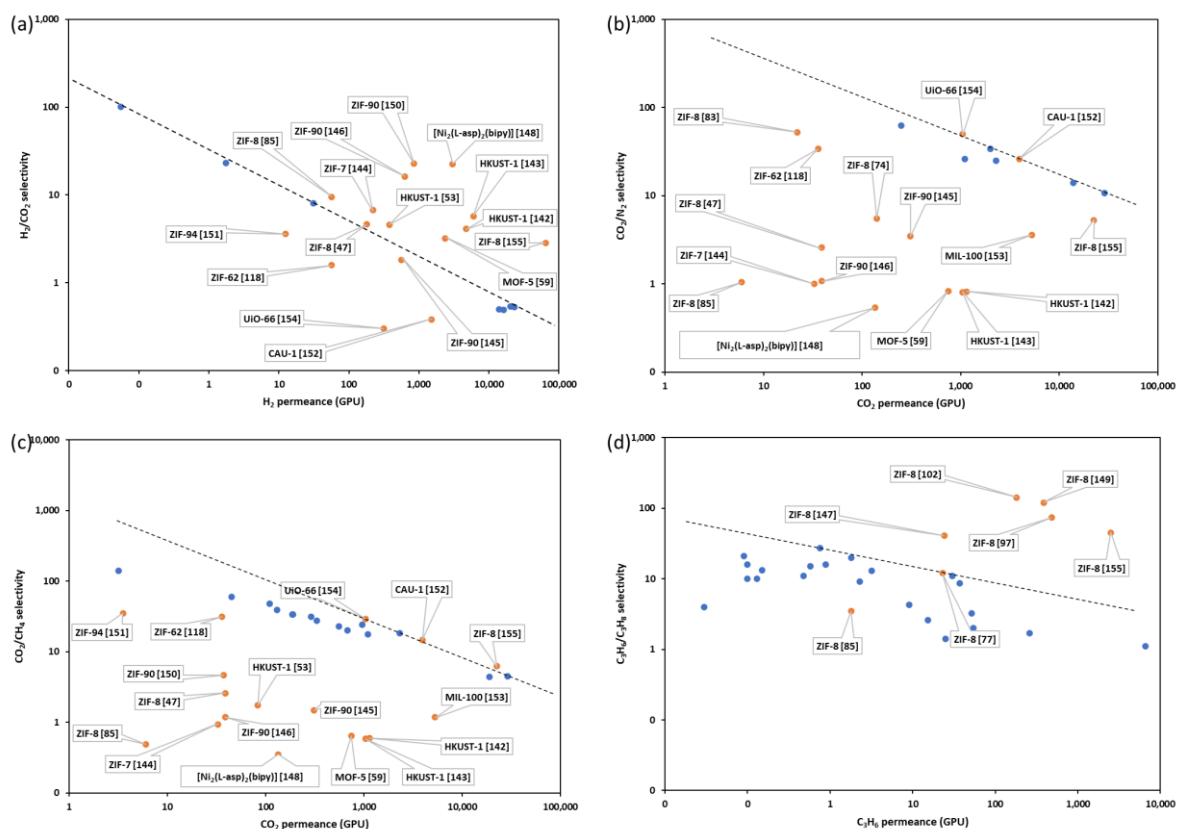


Figure 7. Selectivity-permeance comparisons against upper bounds [156,157]: (a) H_2/CO_2 separation, (b) CO_2/N_2 separation, (c) CO_2/CH_4 separation and (d) $\text{C}_3\text{H}_6/\text{C}_3\text{H}_8$ separation.

Continuous MOF membranes have mostly been used to act as molecular sieves to separate smaller molecules (H_2 , CO_2 , and C_3H_6) from larger molecules (CO_2 , N_2 , CH_4 , and C_3H_8). Excellent hydrogen permeance and selectivity over the upper bound is witnessed in Figure 7a because the electron-poor H_2 is relatively smaller over CO_2 molecules. However, the performance of the CO_2 separation from N_2 and CH_4 using a continuous MOF membrane is below or close to the upper bound, though there is a large difference between the kinetic diameters of CO_2 and N_2 or CH_4 . Apart from the technical factors of membrane production, the window size of the MOF is another factor that might influence the separation performance of CO_2 from N_2 and CH_4 . From Tables 1 and 3, we know the window sizes of ZIF-8 and MIL-96 fall exactly between the kinetic diameters of CO_2 and N_2 or CH_4 . However, it should be noted that some MOFs have a flexible nature and dynamic properties, like the effective aperture size of ZIF-8 between 4.0 to 4.2 Å [158]. That means, the effective aperture sizes of most MOFs in Table 1 are larger than the kinetic diameters of CO_2 , N_2 and CH_4 , resulting in that most continuous MOF membranes cannot exhibit sharp molecular sieving. Furthermore, the interaction, including polarizability, magnetic susceptibility, permanent dipole moment, quadrupole moment, etc. between the gas molecule and the MOF membrane needs to be highly emphasized [159]. From the membrane material aspect, the strong polarizing groups from the MOF ligands such as 1,4-benzenedicarboxylate and imidazolate-2-carboxyaldehyde, and high-valence metal precursors such as Zr^{4+} , Cr^{3+} , Al^{3+} , and Fe^{3+} can make MOF membrane show high adsorption to the gas molecule with a great permanent quadrupole moment, like CO_2 , but strong adsorption can also result in low diffusion coefficients according to recent research [159–161]. Promising molecular sieve performances for the separation of C_3H_6 and C_3H_8 have been witnessed using continuous MOF membranes (Figure 7d). Although reports of $\text{C}_3\text{H}_6/\text{C}_3\text{H}_8$ separation have been limited to ZIF-8, different fabrication methods can lead to different separation performance, such as ZIF-8 [72] and ZIF-8 [142]; even different membrane supports using

the same membrane fabrication method can have different separation performance, such as ZIF-8 [92] and ZIF-8 [150].

Table 3. Kinetic diameter for various molecules.

Molecule	Kinetic Diameter (Å)
H ₂	2.89
CO ₂	3.30
N ₂	3.64
CH ₄	3.80
C ₃ H ₆	3.90
C ₃ H ₈	4.30

3.3. Continuous MOF Membranes in Pervaporation

There are few reports on the continuous MOF membrane being applied in pervaporation, though many continuous MOF membranes have been successfully used for gas separation. In addition to the high requirements for the integrity of the membrane, there are also higher chemical-stability requirements for the membrane, considering that pervaporation is a liquid-phase process. With continuous developments in the field of MOF-based membranes, increasing attention has been paid to the application of continuous MOF membranes in pervaporation. In 2021, Luis et al. published a review on MOF-based membranes in pervaporation [9]. In this review, the design strategies, developments, and performance of continuous MOF membranes were discussed in detail. Compared to other types of membranes, especially polymeric membranes, continuous MOF membranes showed encouraging performance (Table 4 and Figure 8). In the dehydration of organics, SIM membranes exhibited the highest selectivity for the dehydration of EtOH. This can be attributed to the small window of the SIM. The Ni₂(l-asp)₂bipy and UiO-66 had higher water permeances with moderate selectivities because of their larger window sizes. In addition, the hydrophilic surface of the Ni₂(l-asp)₂bipy membrane also contributed to this remarkably high water permeance. In the recovery of organics, the hydrophobicity of ZIF-71 did not endow its corresponding membranes with EtOH selectivity because the small difference between the window size of ZIF-71 and the kinetic diameter of EtOH (Table 5). In the separation of organic–organic mixtures, the window size of UiO-66 (0.60 nm) is far larger than the kinetic diameter of MeOH (0.38 nm), close to that of MTBE (0.62 nm), thus the UiO-66 membrane exhibited the largest MeOH permeance with a moderate selectivity in contrast to the other types of membranes. As it is the same series of the MOF as UiO-66, the polarity of UiO-66-NH₂ is switched from hydrophobicity of UiO-66 to hydrophilicity by grafting amino groups on the organic ligand. The change in the polarity greatly facilitates the adsorption of strongly-polar thiophene [9]. In addition, the kinetic diameter of thiophene (0.46 nm) is much smaller than the window size of UiO-66-NH₂ (0.75 nm), thus it can spread across the membrane by molecular diffusion. That is the reason why the UiO-66-NH₂ membrane showed the highest thiophene permeance and selectivity.

Table 4. Continuous MOF membranes for pervaporation.

MOF	Support	Method	Mixture (i/j)	Mass Ratio (i/j)	T (°C)	Flux (g/m ² ·h)	i Permeance (GPU)	j Permeance (GPU)	Separation Factor ($\beta_{i/j}$)	Selectivity ($\alpha_{i/j}$)	Ref.
CAU-10-H	alumina	secondary growth	H ₂ O/EtOH	10–90	40	397	5391.77	12.52	324	430.61	[162]
CAU-10-H	alumina	secondary growth	H ₂ O/EtOH	10–91	65	493	1914.48	10.63	148	180.09	[162]
Ni ₂ (l-asp) ₂ bipy	SiO ₂	secondary growth	H ₂ O/EtOH	50/50	30	28,100	373,279.57	1169.2	73.6	319.26	[65]
Sm-DOBDC	alumina	secondary growth	H ₂ O/EtOH	5/95	50	786.4	N/A	N/A	>9481	N/A	[129]
SIM-1	glass	mechanical press	H ₂ O/EtOH	55.82/44.18	25	460	10,493.15	0.1589	>10,000	>66,036.24	[119]
UiO-66	Yttria-Stabilized Zirconia	in situ	H ₂ O/EtOH	5/95	50	2550	8776.12	276.85	32.9	31.7	[163]
MIL-96	alumina	secondary growth	H ₂ O/Ethyl acetate	4.4/95.6	60	70	N/A	N/A	>1279	N/A	[61]
UiO-66	alumina	liquid-phase epitaxy	EtOH/H ₂ O	10/90	50	1490	N/A	N/A	4.9	N/A	[164]
ZIF-71	alumina	interfacial synthesis	EtOH/H ₂ O	5–95	25	2601	17,619.83	29,951.78	6.88	0.59	[76]
ZIF-71	ZnO	secondary growth	EtOH/H ₂ O	5–95	25	322.18	1980.52	3833.32	6.07	0.52	[165]
UiO-66	alumina	secondary growth	MeOH/MTBE	5–95	40	1210	2733.36	6.92	597	395.06	[166]
UiO-66	alumina	secondary growth	MeOH/MTBE	15/85	40	1920	2423.83	15.35	147	157.9	[166]
UiO-66-NH ₂	alumina	in situ	Thiophene/n-octane	0.13/99.87	40	2160	~21,000	~4000	17.96 (enrichment factor)	~5.8	[167]

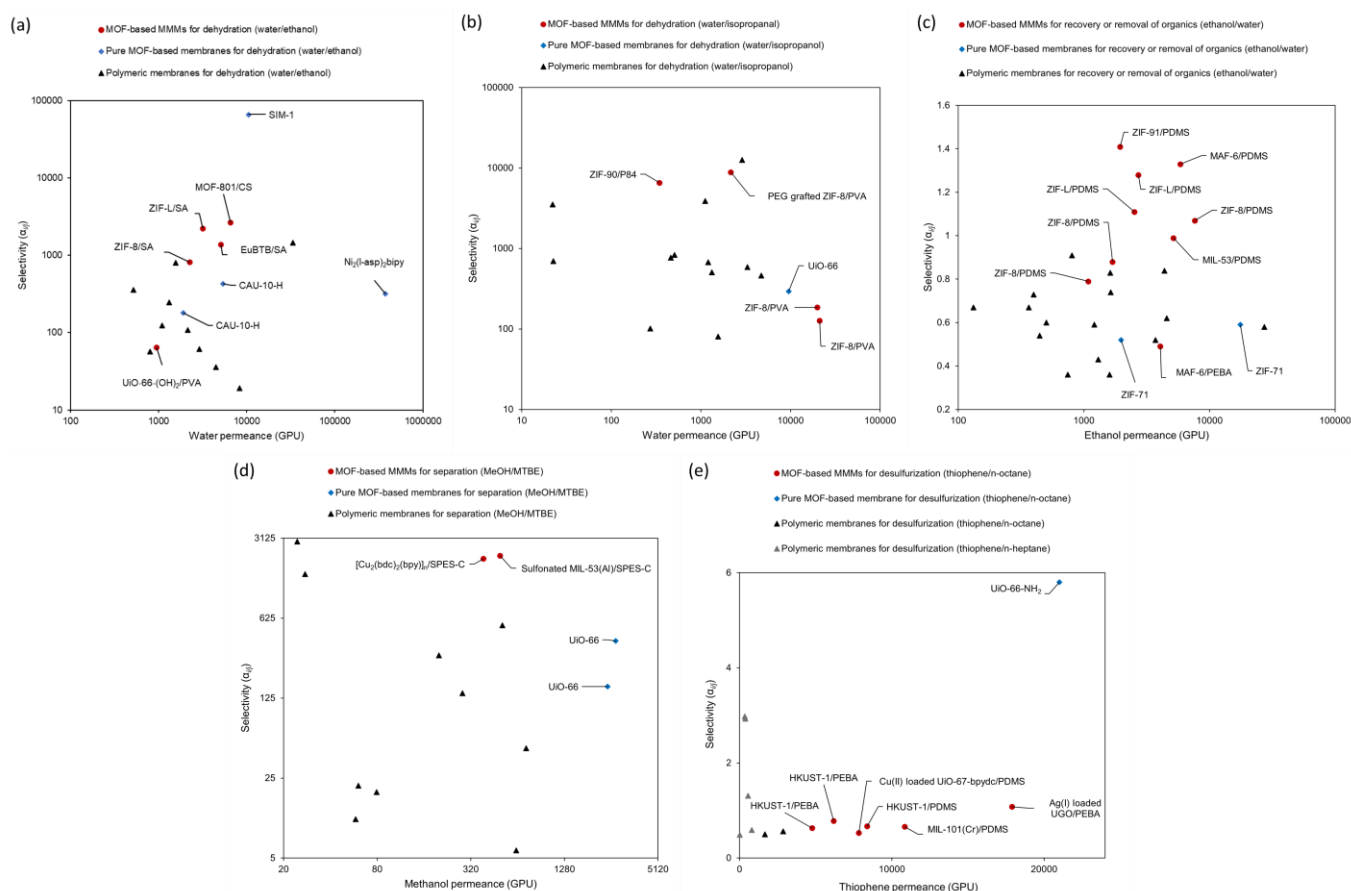


Figure 8. Separation performance of continuous MOF membranes in pervaporation: (a) H₂O/EtOH separation, (b) H₂O/Isopropanol, (c) EtOH/H₂O, (d) MeOH/MTBE and (e) Thiophene/n-octane or n-butane. Reprinted with permission from Ref. [6].

Table 5. Physical parameters of liquid solvents in pervaporation.

Solvent	Kinetic Diameter/Å
Water	2.65
Methanol (MeOH)	3.8
Ethanol (EtOH)	4.3
Isopropanol	4.6
Thiophene	4.6
Methyl tert-butyl ether (MTBE)	6.2
Ethyl acetate	5.2
N-octane	4.3

4. Conclusions and Perspectives

In gas separation and pervaporation, continuous MOF membranes have exhibited promising potentials in pushing the polymer upper bounds. The increasing progress in the continuous MOF membrane is attracting increasing attention. The following issues are recommended to pay attention to in future research: (1) Exploring the membrane fabrication techniques to obtain defect-free continuous MOF membranes; (2) optimizing membrane structures including fabrication parameters, support membrane, and crystal nucleation and growth; (3) characterizing adsorption and desorption behaviours of the gas or liquid molecules accurately in the MOF using effective techniques before practical applications; (4) measuring the effective window size of the MOF for more efficient separations; (5) selecting the suitable MOF for the target application by computational simulation and calculations, not limited to ZIFs; (6) paying more attention to the application

of continuous MOF membranes in pervaporation. Although the application of continuous MOF membranes for gas separation and pervaporation is still in its infancy, we believe that exciting breakthroughs are on the horizon.

Author Contributions: X.X.: Conceptualization, Methodology, Validation, Formal analysis, Investigation, Writing—original draft, Writing—review & editing, Visualization. Y.H.: Conceptualization, Writing—review & editing. J.Z.: Writing—review & editing. P.L.: Writing—review & editing, Supervision. All authors have read and agreed to the published version of the manuscript.

Funding: This research was funded by the China Scholarship Council (CSC), grant number: 201906050060.

Conflicts of Interest: The authors declare no conflict of interest.

References

1. Yong, W.F.; Zhang, H. Recent advances in polymer blend membranes for gas separation and pervaporation. *Prog. Mater. Sci.* **2021**, *116*, 100713. [[CrossRef](#)]
2. Baker, R.W. *Membrane Technology and Applications*; John Wiley & Sons: Hoboken, NJ, USA, 2012.
3. Luis, P. *Fundamental Modeling of Membrane Systems: Membrane and Process Performance*; Elsevier: Amsterdam, The Netherlands, 2018.
4. Zeng, H.; He, S.; Hosseini, S.S.; Zhu, B.; Shao, L. Emerging nanomaterial incorporated membranes for gas separation and pervaporation towards energetic-efficient applications. *Adv. Membr.* **2022**, *2*, 100015. [[CrossRef](#)]
5. Pulyalina, A.; Rostovtseva, V.; Faykov, I.; Tataurov, M.; Dubovenko, R.; Shugurov, S. Development of Novel Polyamide-Imide/DES Composites and Their Application for Pervaporation and Gas Separation. *Molecules* **2021**, *26*, 990. [[CrossRef](#)] [[PubMed](#)]
6. Pandey, P.; Chauhan, R. Membranes for gas separation. *Prog. Polym. Sci.* **2001**, *26*, 853–893. [[CrossRef](#)]
7. Li, W.; Galiano, F.; Estager, J.; Monbaliu, J.-C.M.; Debecker, D.P.; Figoli, A.; Luis, P. Sorption and pervaporation study of methanol/dimethyl carbonate mixture with poly (etheretherketone)(PEEK-WC) membrane. *J. Membr. Sci.* **2018**, *567*, 303–310. [[CrossRef](#)]
8. Qian, Q.; Asinger, P.A.; Lee, M.J.; Han, G.; Mizrahi Rodriguez, K.; Lin, S.; Benedetti, F.M.; Wu, A.X.; Chi, W.S.; Smith, Z.P. MOF-based membranes for gas separations. *Chem. Rev.* **2020**, *120*, 8161–8266. [[CrossRef](#)]
9. Xu, X.; Nikolaeva, D.; Hartanto, Y.; Luis, P. MOF-based membranes for pervaporation. *Sep. Purif. Technol.* **2021**, *278*, 119233.
10. Dai, F.; Luo, J.; Zhou, S.; Qin, X.; Liu, D.; Qi, H. Porous hafnium-containing acid/base bifunctional catalysts for efficient upgrading of bio-derived aldehydes. *J. Bioresour. Bioprod.* **2021**, *6*, 243–253. [[CrossRef](#)]
11. Wang, J.; Sun, Y.; Zhao, X.; Chen, L.; Peng, S.; Ma, C.; Duan, G.; Liu, Z.; Wang, H.; Yuan, Y. A poly (amidoxime)-modified MOF macroporous membrane for high-efficient uranium extraction from seawater. *e-Polymers* **2022**, *22*, 399–410. [[CrossRef](#)]
12. Jian, S.; Ma, X.; Wang, Q.; Wu, J.; Wang, Y.; Jiang, S.; Xu, W.; Yang, W. Hierarchical porous Co₃O₄ nanocages with elaborate microstructures derived from ZIF-67 toward lithium storage. *Vacuum* **2021**, *184*, 109879. [[CrossRef](#)]
13. Caro, J. Are MOF membranes better in gas separation than those made of zeolites? *Curr. Opin. Chem. Eng.* **2011**, *1*, 77–83. [[CrossRef](#)]
14. Shekhah, O.; Chernikova, V.; Belmabkhout, Y.; Eddaoudi, M. Metal–organic framework membranes: From fabrication to gas separation. *Crystals* **2018**, *8*, 412. [[CrossRef](#)]
15. Kang, Z.; Fan, L.; Sun, D. Recent advances and challenges of metal–organic framework membranes for gas separation. *J. Mater. Chem. A* **2017**, *5*, 10073–10091. [[CrossRef](#)]
16. Yang, L.; Qian, S.; Wang, X.; Cui, X.; Chen, B.; Xing, H. Energy-efficient separation alternatives: Metal–organic frameworks and membranes for hydrocarbon separation. *Chem. Soc. Rev.* **2020**, *49*, 5359–5406. [[CrossRef](#)] [[PubMed](#)]
17. Xue, D.-X.; Cadiou, A.; Weseliński, Ł.J.; Jiang, H.; Bhatt, P.M.; Shkurenko, A.; Wojtas, L.; Chen, Z.; Belmabkhout, Y.; Adil, K. Topology meets MOF chemistry for pore-aperture fine tuning: Ftw-MOF platform for energy-efficient separations via adsorption kinetics or molecular sieving. *Chem. Commun.* **2018**, *54*, 6404–6407. [[CrossRef](#)] [[PubMed](#)]
18. Ma, X.; Zhao, S.; Tian, Z.; Duan, G.; Pan, H.; Yue, Y.; Li, S.; Jian, S.; Yang, W.; Liu, K. MOFs meet wood: Reusable magnetic hydrophilic composites toward efficient water treatment with super-high dye adsorption capacity at high dye concentration. *Chem. Eng. J.* **2022**, *446*, 136851. [[CrossRef](#)]
19. Ma, X.; Xiong, Y.; Liu, Y.; Han, J.; Duan, G.; Chen, Y.; He, S.; Mei, C.; Jiang, S.; Zhang, K. When MOFs meet wood: From opportunities toward applications. *Chem* **2022**, *8*, 2342–2361. [[CrossRef](#)]
20. Hermes, S.; Schröder, F.; Chelmowski, R.; Wöll, C.; Fischer, R.A. Selective nucleation and growth of metal-organic open framework thin films on patterned COOH/CF₃-terminated self-assembled monolayers on Au (111). *J. Am. Chem. Soc.* **2005**, *127*, 13744–13745. [[CrossRef](#)]
21. Wang, X.-P.; Hou, J.; Chen, F.-S.; Meng, X.-M. In-situ growth of metal-organic framework film on a polydopamine-modified flexible substrate for antibacterial and forward osmosis membranes. *Sep. Purif. Technol.* **2020**, *236*, 116239. [[CrossRef](#)]
22. Kwon, H.T.; Jeong, H.-K. In situ synthesis of thin zeolitic–imidazolate framework ZIF-8 membranes exhibiting exceptionally high propylene/propane separation. *J. Am. Chem. Soc.* **2013**, *135*, 10763–10768. [[CrossRef](#)]

23. Tuerhong, M.; Nizamidin, P.; Yimit, A.; Simayi, R. In situ growth and optical gas adsorption performance of Zn (II) metal–organic framework membranes at room temperature. *Analyst* **2019**, *144*, 4887–4896. [[CrossRef](#)] [[PubMed](#)]
24. Zhang, J.; Xia, T.; Zhao, D.; Cui, Y.; Yang, Y.; Qian, G. In situ secondary growth of Eu (III)-organic framework film for fluorescence sensing of sulfur dioxide. *Sens. Actuators B Chem.* **2018**, *260*, 63–69. [[CrossRef](#)]
25. Wu, X.; Yang, Y.; Lu, X.; Wang, Z. Seeded growth of high-performance ZIF-8 membranes in thick wall autoclaves assisted by modulator. *J. Membr. Sci.* **2020**, *613*, 118518. [[CrossRef](#)]
26. Ma, X.; Li, Y.; Huang, A. Synthesis of nano-sheets seeds for secondary growth of highly hydrogen permselective ZIF-95 membranes. *J. Membr. Sci.* **2020**, *597*, 117629. [[CrossRef](#)]
27. Wu, W.; Jia, M.; Su, J.; Li, Z.; Li, W. Air–water interfacial synthesis of metal–organic framework hollow fiber membranes for water purification. *AIChE J.* **2020**, *66*, e16238. [[CrossRef](#)]
28. Vatanpour, V.; Khorshidi, S. Surface modification of polyvinylidene fluoride membranes with ZIF-8 nanoparticles layer using interfacial method for BSA separation and dye removal. *Mater. Chem. Phys.* **2020**, *241*, 122400. [[CrossRef](#)]
29. Yao, J.; Wang, H. Zeolitic imidazolate framework composite membranes and thin films: Synthesis and applications. *Chem. Soc. Rev.* **2014**, *43*, 4470–4493. [[CrossRef](#)]
30. Yeo, Z.Y.; Chai, S.-P.; Zhu, P.W.; Mohamed, A.R. An overview: Synthesis of thin films/membranes of metal organic frameworks and its gas separation performances. *RSC Adv.* **2014**, *4*, 54322–54334. [[CrossRef](#)]
31. Zhang, C.; Wu, B.-H.; Ma, M.-Q.; Wang, Z.; Xu, Z.-K. Ultrathin metal/covalent–organic framework membranes towards ultimate separation. *Chem. Soc. Rev.* **2019**, *48*, 3811–3841. [[CrossRef](#)] [[PubMed](#)]
32. Yu, X.-J.; Xian, Y.-M.; Wang, C.; Mao, H.-L.; Kind, M.; Abu-Husein, T.; Chen, Z.; Zhu, S.-B.; Ren, B.; Terfort, A. Liquid-phase epitaxial growth of highly oriented and multivariate surface-attached metal–organic frameworks. *J. Am. Chem. Soc.* **2019**, *141*, 18984–18993. [[CrossRef](#)]
33. Liu, J.; Wöll, C. Surface-supported metal–organic framework thin films: Fabrication methods, applications, and challenges. *Chem. Soc. Rev.* **2017**, *46*, 5730–5770. [[CrossRef](#)] [[PubMed](#)]
34. Eddaoudi, M.; Shekhah, O.; Belmabkhout, Y. Fabrication of Highly CO₂ Selective Metal-Organic Framework Membrane using Liquid Phase Epitaxy Approach. U.S. Patents US20170203261A1, 15 October 2019.
35. Chernikova, V.; Shekhah, O.; Belmabkhout, Y.; Eddaoudi, M. Nanoporous fluorinated metal–organic framework-based membranes for CO₂ capture. *ACS Appl. Nano Mater.* **2020**, *3*, 6432–6439. [[CrossRef](#)]
36. Boscher, N.D.; Wang, M.; Perrotta, A.; Heinze, K.; Creatore, M.; Gleason, K.K. Metal–organic covalent network chemical vapor deposition for gas separation. *Adv. Mater.* **2016**, *28*, 7479–7485. [[CrossRef](#)]
37. Li, W. Metal–organic framework membranes: Production, modification, and applications. *Prog. Mater. Sci.* **2019**, *100*, 21–63. [[CrossRef](#)]
38. Betard, A.; Fischer, R.A. Metal–organic framework thin films: From fundamentals to applications. *Chem. Rev.* **2012**, *112*, 1055–1083. [[CrossRef](#)]
39. Stassen, I.; Styles, M.; Greci, G.; Gorp, H.V.; Vanderlinden, W.; Feyter, S.D.; Falcaro, P.; Vos, D.D.; Vereecken, P.; Ameloot, R. Chemical vapour deposition of zeolitic imidazolate framework thin films. *Nat. Mater.* **2016**, *15*, 304–310. [[CrossRef](#)]
40. Liu, X. Metal-organic framework UiO-66 membranes. *Front. Chem. Sci. Eng.* **2020**, *14*, 216–232. [[CrossRef](#)]
41. Cruz, A.J.; Stassen, I.; Krishtab, M.; Marcoen, K.; Stassin, T.; Rodríguez-Hermida, S.; Teyssandier, J.; Pletincx, S.; Verbeke, R.; Rubio-Giménez, V. Integrated cleanroom process for the vapor-phase deposition of large-area zeolitic imidazolate framework thin films. *Chem. Mater.* **2019**, *31*, 9462–9471. [[CrossRef](#)]
42. Alizadeh, S.; Nematollahi, D. Convergent and divergent paired electrodeposition of metal-organic framework thin films. *Sci. Rep.* **2019**, *9*, 14325. [[CrossRef](#)]
43. Li, M.; Dinca, M. Selective formation of biphasic thin films of metal–organic frameworks by potential-controlled cathodic electrodeposition. *Chem. Sci.* **2014**, *5*, 107–111. [[CrossRef](#)]
44. Liu, H.; Wang, H.; Chu, T.; Yu, M.; Yang, Y. An electrodeposited lanthanide MOF thin film as a luminescent sensor for carbonate detection in aqueous solution. *J. Mater. Chem. C* **2014**, *2*, 8683–8690. [[CrossRef](#)]
45. Lin, Y.S. Metal organic framework membranes for separation applications. *Curr. Opin. Chem. Eng.* **2015**, *8*, 21–28. [[CrossRef](#)]
46. Liu, Y.; Ng, Z.; Khan, E.A.; Jeong, H.-K.; Ching, C.-B.; Lai, Z. Synthesis of continuous MOF-5 membranes on porous α -alumina substrates. *Microporous Mesoporous Mater.* **2009**, *118*, 296–301. [[CrossRef](#)]
47. Bux, H.; Liang, F.; Li, Y.; Cravillon, J.; Wiebcke, M.; Caro, J.R. Zeolitic imidazolate framework membrane with molecular sieving properties by microwave-assisted solvothermal synthesis. *J. Am. Chem. Soc.* **2009**, *131*, 16000–16001. [[CrossRef](#)] [[PubMed](#)]
48. Xu, G.; Yao, J.; Wang, K.; He, L.; Webley, P.A.; Chen, C.-S.; Wang, H. Preparation of ZIF-8 membranes supported on ceramic hollow fibers from a concentrated synthesis gel. *J. Membr. Sci.* **2011**, *385*, 187–193. [[CrossRef](#)]
49. Kang, Z.; Xue, M.; Fan, L.; Ding, J.; Guo, L.; Gao, L.; Qiu, S. “Single nickel source” in situ fabrication of a stable homochiral MOF membrane with chiral resolution properties. *Chem. Commun.* **2013**, *49*, 10569–10571. [[CrossRef](#)]
50. Zhang, X.; Liu, Y.; Kong, L.; Liu, H.; Qiu, J.; Han, W.; Weng, L.-T.; Yeung, K.L.; Zhu, W. A simple and scalable method for preparing low-defect ZIF-8 tubular membranes. *J. Mater. Chem. A* **2013**, *1*, 10635–10638. [[CrossRef](#)]
51. Ma, L.; Svec, F.; Tan, T.; Lv, Y. In-situ growth of highly permeable zeolite imidazolate framework membranes on porous polymer substrate using metal chelated polyaniline as interface layer. *J. Membr. Sci.* **2019**, *576*, 1–8. [[CrossRef](#)]

52. Wu, X.; Wei, W.; Jiang, J.; Caro, J.; Huang, A. High-Flux High-Selectivity Metal–Organic Framework MIL-160 Membrane for Xylene Isomer Separation by Pervaporation. *Angew. Chem. Int. Ed.* **2018**, *57*, 15354–15358. [[CrossRef](#)] [[PubMed](#)]
53. Guo, H.; Zhu, G.; Hewitt, I.J.; Qiu, S. “Twin copper source” growth of metal-organic framework membrane: $\text{Cu}_3(\text{BTC})_2$ with high permeability and selectivity for recycling H_2 . *J. Am. Chem. Soc.* **2009**, *131*, 1646–1647. [[CrossRef](#)]
54. Algieri, C.; Golemme, G.; Kallus, S.; Ramsay, J. Preparation of thin supported MFI membranes by in situ nucleation and secondary growth. *Microporous Mesoporous Mater.* **2001**, *47*, 127–134. [[CrossRef](#)]
55. Snyder, M.A.; Tsapatsis, M. Hierarchical nanomanufacturing: From shaped zeolite nanoparticles to high-performance separation membranes. *Angew. Chem. Int. Ed.* **2007**, *46*, 7560–7573. [[CrossRef](#)] [[PubMed](#)]
56. Bohrman, J.A.; Carreon, M.A. Synthesis and CO_2/CH_4 separation performance of Bio-MOF-1 membranes. *Chem. Commun.* **2012**, *48*, 5130–5132. [[CrossRef](#)]
57. Pan, Y.; Li, T.; Lestari, G.; Lai, Z. Effective separation of propylene/propane binary mixtures by ZIF-8 membranes. *J. Membr. Sci.* **2012**, *390*, 93–98. [[CrossRef](#)]
58. Wu, Y.-N.; Li, F.; Liu, H.; Zhu, W.; Teng, M.; Jiang, Y.; Li, W.; Xu, D.; He, D.; Hannam, P. Electrospun fibrous mats as skeletons to produce free-standing MOF membranes. *J. Mater. Chem.* **2012**, *22*, 16971–16978. [[CrossRef](#)]
59. Yoo, Y.; Lai, Z.; Jeong, H.-K. Fabrication of MOF-5 membranes using microwave-induced rapid seeding and solvothermal secondary growth. *Microporous Mesoporous Mater.* **2009**, *123*, 100–106. [[CrossRef](#)]
60. Hu, Y.; Wei, J.; Liang, Y.; Zhang, H.; Zhang, X.; Shen, W.; Wang, H. Zeolitic imidazolate framework/graphene oxide hybrid nanosheets as seeds for the growth of ultrathin molecular sieving membranes. *Angew. Chem.* **2016**, *128*, 2088–2092. [[CrossRef](#)]
61. Hu, Y.; Dong, X.; Nan, J.; Jin, W.; Ren, X.; Xu, N.; Lee, Y.M. Metal–organic framework membranes fabricated via reactive seeding. *Chem. Commun.* **2011**, *47*, 737–739. [[CrossRef](#)]
62. Guerrero, V.V.; Yoo, Y.; McCarthy, M.C.; Jeong, H.-K. HKUST-1 membranes on porous supports using secondary growth. *J. Mater. Chem.* **2010**, *20*, 3938–3943. [[CrossRef](#)]
63. Ranjan, R.; Tsapatsis, M. Microporous metal organic framework membrane on porous support using the seeded growth method. *Chem. Mater.* **2009**, *21*, 4920–4924. [[CrossRef](#)]
64. Pan, Y.; Wang, B.; Lai, Z. Synthesis of ceramic hollow fiber supported zeolitic imidazolate framework-8 (ZIF-8) membranes with high hydrogen permeability. *J. Membr. Sci.* **2012**, *421*, 292–298. [[CrossRef](#)]
65. Wang, S.; Kang, Z.; Xu, B.; Fan, L.; Li, G.; Wen, L.; Xin, X.; Xiao, Z.; Pang, J.; Du, X. Wettability switchable metal-organic framework membranes for pervaporation of water/ethanol mixtures. *Inorg. Chem. Commun.* **2017**, *82*, 64–67. [[CrossRef](#)]
66. Diestel, L.; Bux, H.; Wachsmuth, D.; Caro, J. Pervaporation studies of n-hexane, benzene, mesitylene and their mixtures on zeolitic imidazolate framework-8 membranes. *Microporous Mesoporous Mater.* **2012**, *164*, 288–293. [[CrossRef](#)]
67. Tao, K.; Kong, C.; Chen, L. High performance ZIF-8 molecular sieve membrane on hollow ceramic fiber via crystallizing-rubbing seed deposition. *Chem. Eng. J.* **2013**, *220*, 1–5. [[CrossRef](#)]
68. Lee, M.J.; Hamid, M.R.A.; Lee, J.; Kim, J.S.; Lee, Y.M.; Jeong, H.-K. Ultrathin zeolitic-imidazolate framework ZIF-8 membranes on polymeric hollow fibers for propylene/propane separation. *J. Membr. Sci.* **2018**, *559*, 28–34. [[CrossRef](#)]
69. Zhao, X.; Zhang, H.; Xu, S.; Wang, Y. ZIF-8 membrane synthesized via covalent-assisted seeding on polyimide substrate for pervaporation dehydration. *AIChE J.* **2019**, *65*, e16620. [[CrossRef](#)]
70. Liu, Y.; Ban, Y.; Yang, W. Microstructural engineering and architectural design of metal–organic framework membranes. *Adv. Mater.* **2017**, *29*, 1606949. [[CrossRef](#)] [[PubMed](#)]
71. Ameloot, R.; Vermoortele, F.; Vanhove, W.; Roeyfaers, M.B.; Sels, B.F.; De Vos, D.E. Interfacial synthesis of hollow metal–organic framework capsules demonstrating selective permeability. *Nat. Chem.* **2011**, *3*, 382–387. [[CrossRef](#)] [[PubMed](#)]
72. Yao, J.; Dong, D.; Li, D.; He, L.; Xu, G.; Wang, H. Contra-diffusion synthesis of ZIF-8 films on a polymer substrate. *Chem. Commun.* **2011**, *47*, 2559–2561. [[CrossRef](#)]
73. Lu, H.; Zhu, S. Interfacial Synthesis of Free-Standing Metal–Organic Framework Membranes. *Eur. J. Inorg. Chem.* **2013**, *2013*, 1294–1300. [[CrossRef](#)]
74. Chen, S.S.; Yang, Z.-J.; Chang, C.-H.; Koh, H.-U.; Al-Saeedi, S.I.; Tung, K.-L.; Wu, K.C.-W. Interfacial nanoarchitectonics for ZIF-8 membranes with enhanced gas separation. *Beilstein J. Nanotechnol.* **2022**, *13*, 313–324. [[CrossRef](#)] [[PubMed](#)]
75. He, M.; Yao, J.; Li, L.; Zhong, Z.; Chen, F.; Wang, H. Aqueous solution synthesis of ZIF-8 films on a porous nylon substrate by contra-diffusion method. *Microporous Mesoporous Mater.* **2013**, *179*, 10–16. [[CrossRef](#)]
76. Huang, K.; Li, Q.; Liu, G.; Shen, J.; Guan, K.; Jin, W. A ZIF-71 hollow fiber membrane fabricated by contra-diffusion. *ACS Appl. Mater. Interfaces* **2015**, *7*, 16157–16160. [[CrossRef](#)] [[PubMed](#)]
77. Brown, A.J.; Brunelli, N.A.; Eum, K.; Rashidi, F.; Johnson, J.; Koros, W.J.; Jones, C.W.; Nair, S. Interfacial microfluidic processing of metal-organic framework hollow fiber membranes. *Science* **2014**, *345*, 72–75. [[CrossRef](#)]
78. Peng, Y.; Li, Y.; Ban, Y.; Jin, H.; Jiao, W.; Liu, X.; Yang, W. Metal-organic framework nanosheets as building blocks for molecular sieving membranes. *Science* **2014**, *346*, 1356–1359. [[CrossRef](#)]
79. Shen, J.; Liu, G.; Huang, K.; Chu, Z.; Jin, W.; Xu, N. Subnanometer two-dimensional graphene oxide channels for ultrafast gas sieving. *ACS Nano* **2016**, *10*, 3398–3409. [[CrossRef](#)]
80. Zhang, S.; Wang, Z.; Ren, H.; Zhang, F.; Jin, J. Nanoporous film-mediated growth of ultrathin and continuous metal–organic framework membranes for high-performance hydrogen separation. *J. Mater. Chem. A* **2017**, *5*, 1962–1966. [[CrossRef](#)]

81. Huang, K.; Dong, Z.; Li, Q.; Jin, W. Growth of a ZIF-8 membrane on the inner-surface of a ceramic hollow fiber via cycling precursors. *Chem. Commun.* **2013**, *49*, 10326–10328. [[CrossRef](#)]
82. Cacho-Bailo, F.; Caro, G.; Etxeberria-Benavides, M.; Karvan, O.; Téllez, C.; Coronas, J. High selectivity ZIF-93 hollow fiber membranes for gas separation. *Chem. Commun.* **2015**, *51*, 11283–11285. [[CrossRef](#)]
83. Marti, A.M.; Wickramanayake, W.; Dahe, G.; Sekizkardes, A.; Bank, T.L.; Hopkinson, D.P.; Venna, S.R. Continuous flow processing of ZIF-8 membranes on polymeric porous hollow fiber supports for CO₂ capture. *ACS Appl. Mater. Interfaces* **2017**, *9*, 5678–5682. [[CrossRef](#)]
84. Shekhah, O.; Wang, H.; Strunskus, T.; Cyganik, P.; Zacher, D.; Fischer, R.; Wöll, C. Layer-by-layer growth of oriented metal organic polymers on a functionalized organic surface. *Langmuir* **2007**, *23*, 7440–7442. [[CrossRef](#)] [[PubMed](#)]
85. Shekhah, O.; Swaidan, R.; Belmabkhout, Y.; Du Plessis, M.; Jacobs, T.; Barbour, L.J.; Pinnau, I.; Eddaoudi, M. The liquid phase epitaxy approach for the successful construction of ultra-thin and defect-free ZIF-8 membranes: Pure and mixed gas transport study. *Chem. Commun.* **2014**, *50*, 2089–2092. [[CrossRef](#)] [[PubMed](#)]
86. Arslan, H.K.; Shekhah, O.; Wohlgemuth, J.; Franzreb, M.; Fischer, R.A.; Wöll, C. High-Throughput Fabrication of Uniform and Homogenous MOF Coatings. *Adv. Funct. Mater.* **2011**, *21*, 4228–4231. [[CrossRef](#)]
87. Gu, Z.-G.; Pfriem, A.; Hamsch, S.; Breitwieser, H.; Wohlgemuth, J.; Heinke, L.; Gliemann, H.; Wöll, C. Transparent films of metal-organic frameworks for optical applications. *Microporous Mesoporous Mater.* **2015**, *211*, 82–87. [[CrossRef](#)]
88. Shekhah, O.; Wang, H.; Kowarik, S.; Schreiber, F.; Paulus, M.; Tolan, M.; Sternemann, C.; Evers, F.; Zacher, D.; Fischer, R.A. Step-by-step route for the synthesis of metal-organic frameworks. *J. Am. Chem. Soc.* **2007**, *129*, 15118–15119. [[CrossRef](#)] [[PubMed](#)]
89. Valadez Sánchez, E.P.; Gliemann, H.; Haas-Santo, K.; Wöll, C.; Dittmeyer, R. ZIF-8 SURMOF Membranes Synthesized by Au-Assisted Liquid Phase Epitaxy for Application in Gas Separation. *Chem. Ing. Tech.* **2016**, *88*, 1798–1805. [[CrossRef](#)]
90. Hashem, T.; Valadez Sánchez, E.P.; Weidler, P.G.; Gliemann, H.; Alkordi, M.H.; Wöll, C. Liquid-Phase Quasi-Epitaxial Growth of Highly Stable, Monolithic UiO-66-NH₂ MOF thin Films on Solid Substrates. *ChemistryOpen* **2020**, *9*, 524–527. [[CrossRef](#)]
91. Micero, A.; Hashem, T.; Gliemann, H.; Léon, A. Hydrogen Separation Performance of UiO-66-NH₂ Membranes Grown via Liquid-Phase Epitaxy Layer-by-Layer Deposition and One-Pot Synthesis. *Membranes* **2021**, *11*, 735. [[CrossRef](#)]
92. Stassen, I.; De Vos, D.; Ameloot, R. Vapor-Phase Deposition and Modification of Metal–Organic Frameworks: State-of-the-Art and Future Directions. *Chem. A Eur. J.* **2016**, *22*, 14452–14460. [[CrossRef](#)]
93. Bennett, T.D.; Cheetham, A.K. Amorphous metal–organic frameworks. *Acc. Chem. Res.* **2014**, *47*, 1555–1562. [[CrossRef](#)]
94. Fischer, D.; von Mankowski, A.; Ranft, A.; Vasa, S.K.; Linser, R.; Mannhart, J.; Lotsch, B.V. ZIF-8 films prepared by femtosecond pulsed-laser deposition. *Chem. Mater.* **2017**, *29*, 5148–5155. [[CrossRef](#)]
95. Ritala, M.; Parala, H.; Kanjolia, R.; Dupuis, R.D.; Alexandrov, S.; Irvine, S.J.; Palgrave, R.; Parkin, I.P.; Niinisto, J.; Krumdieck, S. *Chemical Vapour Deposition: Precursors, Processes and Applications*; Royal Society of Chemistry: London, UK, 2008.
96. Salmi, L.D.; Heikkilä, M.J.; Puukilainen, E.; Sajavaara, T.; Grosso, D.; Ritala, M. Studies on atomic layer deposition of MOF-5 thin films. *Microporous Mesoporous Mater.* **2013**, *182*, 147–154. [[CrossRef](#)]
97. Ma, X.; Kumar, P.; Mittal, N.; Khlyustova, A.; Daoutidis, P.; Mkhoyan, K.A.; Tsapatsis, M. Zeolitic imidazolate framework membranes made by ligand-induced permselectation. *Science* **2018**, *361*, 1008–1011. [[CrossRef](#)] [[PubMed](#)]
98. Lausund, K.B.; Petrovic, V.; Nilsen, O. All-gas-phase synthesis of amino-functionalized UiO-66 thin films. *Dalton Trans.* **2017**, *46*, 16983–16992. [[CrossRef](#)] [[PubMed](#)]
99. Lausund, K.B.; Olsen, M.S.; Hansen, P.-A.; Valen, H.; Nilsen, O. MOF thin films with bi-aromatic linkers grown by molecular layer deposition. *J. Mater. Chem. A* **2020**, *8*, 2539–2548. [[CrossRef](#)]
100. Multia, J.; Karppinen, M. Atomic/Molecular Layer Deposition for Designer’s Functional Metal–Organic Materials. *Adv. Mater. Interfaces* **2022**, *9*, 2200210. [[CrossRef](#)]
101. Li, W.; Su, P.; Li, Z.; Xu, Z.; Wang, F.; Ou, H.; Zhang, J.; Zhang, G.; Zeng, E. Ultrathin metal–organic framework membrane production by gel–vapour deposition. *Nat. Commun.* **2017**, *8*, 406. [[CrossRef](#)]
102. Wei, R.; Chi, H.Y.; Li, X.; Lu, D.; Wan, Y.; Yang, C.W.; Lai, Z. Aqueously cathodic deposition of ZIF-8 membranes for superior propylene/propane separation. *Adv. Funct. Mater.* **2020**, *30*, 1907089. [[CrossRef](#)]
103. Van de Voorde, B.; Ameloot, R.; Stassen, I.; Everaert, M.; De Vos, D.; Tan, J.-C. Mechanical properties of electrochemically synthesised metal–organic framework thin films. *J. Mater. Chem. C* **2013**, *1*, 7716–7724. [[CrossRef](#)]
104. Li, W.-J.; Tu, M.; Cao, R.; Fischer, R.A. Metal–organic framework thin films: Electrochemical fabrication techniques and corresponding applications & perspectives. *J. Mater. Chem. A* **2016**, *4*, 12356–12369.
105. Hod, I.; Bury, W.; Karlin, D.M.; Deria, P.; Kung, C.W.; Katz, M.J.; So, M.; Klahr, B.; Jin, D.; Chung, Y.W. Directed growth of electroactive metal-organic framework thin films using electrophoretic deposition. *Adv. Mater.* **2014**, *26*, 6295–6300. [[CrossRef](#)] [[PubMed](#)]
106. Czaja, A.U.; Trukhan, N.; Müller, U. Industrial applications of metal–organic frameworks. *Chem. Soc. Rev.* **2009**, *38*, 1284–1293. [[CrossRef](#)] [[PubMed](#)]
107. Mueller, U.; Puetter, H.; Hesse, M.; Schubert, M.; Wessel, H.; Huff, J.; Guzman, M. Method for Electrochemical Production of a Crystalline Porous Metal Organic Skeleton Material. U.S. Patents US7968739B2, 28 June 2011.
108. Campagnol, N.; Souza, E.R.; De Vos, D.E.; Binnemans, K.; Franssaer, J. Luminescent terbium-containing metal–organic framework films: New approaches for the electrochemical synthesis and application as detectors for explosives. *Chem. Commun.* **2014**, *50*, 12545–12547. [[CrossRef](#)] [[PubMed](#)]

109. Cheng, K.-Y.; Wang, J.-C.; Lin, C.-Y.; Lin, W.-R.; Chen, Y.-A.; Tsai, F.-J.; Chuang, Y.-C.; Lin, G.-Y.; Ni, C.-W.; Zeng, Y.-T. Electrochemical synthesis, characterization of Ir–Zn containing coordination polymer, and application in oxygen and glucose sensing. *Dalton Trans.* **2014**, *43*, 6536–6547. [[CrossRef](#)]
110. Worrall, S.D.; Mann, H.; Rogers, A.; Bissett, M.A.; Atfield, M.P.; Dryfe, R.A. Electrochemical deposition of zeolitic imidazolate framework electrode coatings for supercapacitor electrodes. *Electrochim. Acta* **2016**, *197*, 228–240. [[CrossRef](#)]
111. Suttipat, D.; Butcha, S.; Assavapanumat, S.; Maihom, T.; Gupta, B.; Perro, A.; Sojic, N.; Kuhn, A.; Wattanakit, C. Chiral macroporous MOF surfaces for electroassisted enantioselective adsorption and separation. *ACS Appl. Mater. Interfaces* **2020**, *12*, 36548–36557. [[CrossRef](#)]
112. Van Assche, T.R.; Denayer, J.F. Fabrication and separation performance evaluation of a metal–organic framework based microseparator device. *Chem. Eng. Sci.* **2013**, *95*, 65–72. [[CrossRef](#)]
113. Campagnol, N.; Van Assche, T.R.; Li, M.; Stappers, L.; Dincă, M.; Denayer, J.F.; Binnemans, K.; De Vos, D.E.; Franssaer, J. On the electrochemical deposition of metal–organic frameworks. *J. Mater. Chem. A* **2016**, *4*, 3914–3925. [[CrossRef](#)]
114. Hauser, J.L.; Tso, M.; Fitchmun, K.; Oliver, S.R. Anodic electrodeposition of several metal organic framework thin films on indium tin oxide glass. *Cryst. Growth Des.* **2019**, *19*, 2358–2365. [[CrossRef](#)]
115. Ameloot, R.; Stappers, L.; Franssaer, J.; Alaerts, L.; Sels, B.F.; De Vos, D.E. Patterned growth of metal-organic framework coatings by electrochemical synthesis. *Chem. Mater.* **2009**, *21*, 2580–2582. [[CrossRef](#)]
116. Li, M.; Dinca, M. Reductive electrosynthesis of crystalline metal–organic frameworks. *J. Am. Chem. Soc.* **2011**, *133*, 12926–12929. [[CrossRef](#)] [[PubMed](#)]
117. Zhu, H.; Liu, H.; Zhitomirsky, I.; Zhu, S. Preparation of metal–organic framework films by electrophoretic deposition method. *Mater. Lett.* **2015**, *142*, 19–22. [[CrossRef](#)]
118. Wang, Y.; Jin, H.; Ma, Q.; Mo, K.; Mao, H.; Feldhoff, A.; Cao, X.; Li, Y.; Pan, F.; Jiang, Z. A MOF glass membrane for gas separation. *Angew. Chem.* **2020**, *132*, 4395–4399. [[CrossRef](#)]
119. Marti, A.M.; Tran, D.; Balkus, K.J. Fabrication of a Substituted Imidazolate Material 1 (SIM-1) membrane using post synthetic modification (PSM) for pervaporation of water/ethanol mixtures. *J. Porous Mater.* **2015**, *22*, 1275–1284. [[CrossRef](#)]
120. Nath, K.; Ahmed, A.; Siegel, D.J.; Matzger, A.J. Microscale Determination of Binary Gas Adsorption Isotherms in MOFs. *J. Am. Chem. Soc.* **2022**, *144*, 20939–20946. [[CrossRef](#)] [[PubMed](#)]
121. Kundu, A.; Sillar, K.; Sauer, J. Ab initio prediction of adsorption isotherms for gas mixtures by Grand Canonical Monte Carlo simulations on a lattice of sites. *J. Phys. Chem. Lett.* **2017**, *8*, 2713–2718. [[CrossRef](#)]
122. Kundu, A.; Sillar, K.; Sauer, J. Predicting adsorption selectivities from pure gas isotherms for gas mixtures in metal–organic frameworks. *Chem. Sci.* **2020**, *11*, 643–655. [[CrossRef](#)]
123. Hou, Q.; Zhou, S.; Wei, Y.; Caro, J.R.; Wang, H. Balancing the grain boundary structure and the framework flexibility through bimetallic Metal–Organic Framework (MOF) membranes for gas separation. *J. Am. Chem. Soc.* **2020**, *142*, 9582–9586. [[CrossRef](#)]
124. Wiersum, A.D.; Chang, J.-S.; Serre, C.; Llewellyn, P.L. An adsorbent performance indicator as a first step evaluation of novel sorbents for gas separations: Application to metal–organic frameworks. *Langmuir* **2013**, *29*, 3301–3309. [[CrossRef](#)]
125. Furukawa, H.; Ko, N.; Go, Y.B.; Aratani, N.; Choi, S.B.; Choi, E.; Yazaydin, A.Ö.; Snurr, R.Q.; O’Keeffe, M.; Kim, J. Ultrahigh porosity in metal-organic frameworks. *Science* **2010**, *329*, 424–428. [[CrossRef](#)]
126. Thornton, A.W.; Dubbeldam, D.; Liu, M.S.; Ladewig, B.P.; Hill, A.J.; Hill, M.R. Feasibility of zeolitic imidazolate framework membranes for clean energy applications. *Energy Environ. Sci.* **2012**, *5*, 7637–7646. [[CrossRef](#)]
127. Reinsch, H.; van der Veen, M.A.; Gil, B.; Marszalek, B.; Verbiest, T.; De Vos, D.; Stock, N. Structures, sorption characteristics, and nonlinear optical properties of a new series of highly stable aluminum MOFs. *Chem. Mater.* **2013**, *25*, 17–26. [[CrossRef](#)]
128. Cuadrado-Collados, C.; Fernández-Català, J.; Fauth, F.; Cheng, Y.Q.; Daemen, L.L.; Ramirez-Cuesta, A.J.; Silvestre-Albero, J. Understanding the breathing phenomena in nano-ZIF-7 upon gas adsorption. *J. Mater. Chem. A* **2017**, *5*, 20938–20946. [[CrossRef](#)]
129. Zhai, L.; Yu, X.; Wang, Y.; Zhang, J.; Ying, Y.; Cheng, Y.; Peh, S.B.; Liu, G.; Wang, X.; Cai, Y. Polycrystalline rare-earth metal-organic framework membranes with in-situ healing ability for efficient alcohol dehydration. *J. Membr. Sci.* **2020**, *610*, 118239. [[CrossRef](#)]
130. Marti, A.M.; Van, M.; Balkus, K.J. Tuning the crystal size and morphology of the substituted imidazole material, SIM-1. *J. Porous Mater.* **2014**, *21*, 889–902. [[CrossRef](#)]
131. Sabetghadam, A.; Liu, X.; Benzaqui, M.; Gkaniatsou, E.; Orsi, A.; Lozinska, M.M.; Sicard, C.; Johnson, T.; Steunou, N.; Wright, P.A. Influence of Filler Pore Structure and Polymer on the Performance of MOF-Based Mixed-Matrix Membranes for CO₂ Capture. *Chem. A Eur. J.* **2018**, *24*, 7949–7956. [[CrossRef](#)]
132. Song, S.; Liu, C.; Ding, R.; Gao, X.; Wang, M.; Li, Z.; Zhao, X. Isomeric Al-BDC-NH₂ metal-organic frameworks for metronidazole removal: Effect of topology structure. *J. Solid State Chem.* **2022**, *314*, 123376. [[CrossRef](#)]
133. Zhang, F.; Zou, X.; Feng, W.; Zhao, X.; Jing, X.; Sun, F.; Ren, H.; Zhu, G. Microwave-assisted crystallization inclusion of spiropyran molecules in indium trimesate films with antidromic reversible photochromism. *J. Mater. Chem.* **2012**, *22*, 25019–25026. [[CrossRef](#)]
134. Frentzel-Beyme, L.; Kolodzeiski, P.; Weiß, J.-B.; Schneemann, A.; Henke, S. Quantification of gas-accessible microporosity in metal-organic framework glasses. *ChemRxiv* **2022**. [[CrossRef](#)]
135. Gandara-Loe, J.; Bueno-Perez, R.; Missyul, A.; Fairen-Jimenez, D.; Silvestre-Albero, J. Molecular Sieving Properties of Nanoporous Mixed-Linker ZIF-62: Associated Structural Changes upon Gas Adsorption Application. *ACS Appl. Nano Mater.* **2021**, *4*, 3519–3528. [[CrossRef](#)]

136. Vaidhyanathan, R.; Bradshaw, D.; Rebilly, J.N.; Barrio, J.P.; Gould, J.A.; Berry, N.G.; Rosseinsky, M.J. A family of nanoporous materials based on an amino acid backbone. *Angew. Chem. Int. Ed.* **2006**, *45*, 6495–6499. [[CrossRef](#)] [[PubMed](#)]
137. Akpınar, I.; Drout, R.J.; Islamoglu, T.; Kato, S.; Lyu, J.; Farha, O.K. Exploiting π - π interactions to design an efficient sorbent for atrazine removal from water. *ACS Appl. Mater. Interfaces* **2019**, *11*, 6097–6103. [[CrossRef](#)] [[PubMed](#)]
138. DMello, M.E.; Sundaram, N.G.; Singh, A.; Singh, A.K.; Kalidindi, S.B. An amine functionalized zirconium metal-organic framework as an effective chemiresistive sensor for acidic gases. *Chem. Commun.* **2019**, *55*, 349–352. [[CrossRef](#)] [[PubMed](#)]
139. Abid, H.R.; Rada, Z.H.; Li, Y.; Mohammed, H.A.; Wang, Y.; Wang, S.; Arandiyani, H.; Tan, X.; Liu, S. Boosting CO₂ adsorption and selectivity in metal-organic frameworks of MIL-96 (Al) via second metal Ca coordination. *RSC Adv.* **2020**, *10*, 8130–8139. [[CrossRef](#)]
140. Benzaqui, M.; Pillai, R.S.; Sabetghadam, A.; Benoit, V.; Normand, P.; Marrot, J.; Menguy, N.; Montero, D.; Shepard, W.; Tissot, A. Revisiting the aluminum trimesate-based MOF (MIL-96): From structure determination to the processing of mixed matrix membranes for CO₂ capture. *Chem. Mater.* **2017**, *29*, 10326–10338. [[CrossRef](#)]
141. Chowdhury, P.; Mekala, S.; Dreisbach, F.; Gumma, S. Adsorption of CO, CO₂ and CH₄ on Cu-BTC and MIL-101 metal organic frameworks: Effect of open metal sites and adsorbate polarity. *Microporous Mesoporous Mater.* **2012**, *152*, 246–252. [[CrossRef](#)]
142. Mao, Y.; Huang, H.; Cao, W.; Li, J.; Sun, L.; Jin, X.; Peng, X. Room temperature synthesis of free-standing HKUST-1 membranes from copper hydroxide nanostrands for gas separation. *Chem. Commun.* **2013**, *49*, 5666–5668. [[CrossRef](#)]
143. Mao, Y.; Li, J.; Cao, W.; Ying, Y.; Sun, L.; Peng, X. Pressure-assisted synthesis of HKUST-1 thin film on polymer hollow fiber at room temperature toward gas separation. *ACS Appl. Mater. Interfaces* **2014**, *6*, 4473–4479. [[CrossRef](#)]
144. Li, Y.S.; Liang, F.Y.; Bux, H.; Feldhoff, A.; Yang, W.S.; Caro, J. Molecular sieve membrane: Supported metal-organic framework with high hydrogen selectivity. *Angew. Chem.* **2010**, *122*, 558–561. [[CrossRef](#)]
145. Huang, A.; Wang, N.; Kong, C.; Caro, J. Organosilica-functionalized zeolitic imidazolate framework ZIF-90 membrane with high gas-separation performance. *Angew. Chem.* **2012**, *124*, 10703–10707. [[CrossRef](#)]
146. Huang, A.; Caro, J. Covalent post-functionalization of zeolitic imidazolate framework ZIF-90 membrane for enhanced hydrogen selectivity. *Angew. Chem. Int. Ed.* **2011**, *50*, 4979–4982. [[CrossRef](#)] [[PubMed](#)]
147. Shah, M.N.; Gonzalez, M.A.; McCarthy, M.C.; Jeong, H.-K. An unconventional rapid synthesis of high performance metal-organic framework membranes. *Langmuir* **2013**, *29*, 7896–7902. [[CrossRef](#)] [[PubMed](#)]
148. Kang, Z.; Fan, L.; Wang, S.; Sun, D.; Xue, M.; Qiu, S. In situ confinement of free linkers within a stable MOF membrane for highly improved gas separation properties. *CrystEngComm* **2017**, *19*, 1601–1606. [[CrossRef](#)]
149. Wang, J.; Wang, Y.; Liu, Y.; Wu, H.; Zhao, M.; Ren, Y.; Pu, Y.; Li, W.; Wang, S.; Song, S. Ultrathin ZIF-8 Membrane through Inhibited Ostwald Ripening for High-Flux C₃H₆/C₃H₈ Separation. *Adv. Funct. Mater.* **2022**, *32*, 2208064. [[CrossRef](#)]
150. Huang, A.; Liu, Q.; Wang, N.; Caro, J. Organosilica functionalized zeolitic imidazolate framework ZIF-90 membrane for CO₂/CH₄ separation. *Microporous Mesoporous Mater.* **2014**, *192*, 18–22. [[CrossRef](#)]
151. Cacho-Bailo, F.; Etxebarria-Benavides, M.; Karvan, O.; Téllez, C.; Coronas, J. Sequential amine functionalization inducing structural transition in an aldehyde-containing zeolitic imidazolate framework: Application to gas separation membranes. *CrystEngComm* **2017**, *19*, 1545–1554. [[CrossRef](#)]
152. Yin, H.; Wang, J.; Xie, Z.; Yang, J.; Bai, J.; Lu, J.; Zhang, Y.; Yin, D.; Lin, J.Y. A highly permeable and selective amino-functionalized MOF CAU-1 membrane for CO₂-N₂ separation. *Chem. Commun.* **2014**, *50*, 3699–3701. [[CrossRef](#)]
153. Dou, Z.; Cai, J.; Cui, Y.; Yu, J.; Xia, T.; Yang, Y.; Qian, G. Preparation and Gas Separation Properties of Metal-Organic Framework Membranes. *Z. Anorg. Allg. Chem.* **2015**, *641*, 792–796. [[CrossRef](#)]
154. Wu, W.; Li, Z.; Chen, Y.; Li, W. Polydopamine-modified metal-organic framework membrane with enhanced selectivity for carbon capture. *Environ. Sci. Technol.* **2019**, *53*, 3764–3772. [[CrossRef](#)]
155. Liu, Y.; Wang, S.; Liu, H.; Peng, L.-M. Carbon nanotube-based three-dimensional monolithic optoelectronic integrated system. *Nat. Commun.* **2017**, *8*, 15649. [[CrossRef](#)]
156. Robeson, L.M. The upper bound revisited. *J. Membr. Sci.* **2008**, *320*, 390–400. [[CrossRef](#)]
157. Burns, R.L.; Koros, W.J. Defining the challenges for C₃H₆/C₃H₈ separation using polymeric membranes. *J. Membr. Sci.* **2003**, *211*, 299–309. [[CrossRef](#)]
158. Xu, X.; Hartanto, Y.; Nikolaeva, D.; He, Z.; Chergaoui, S.; Luis, P. High-performance ZIF-8/biopolymer chitosan mixed-matrix pervaporation membrane for methanol/dimethyl carbonate separation. *Sep. Purif. Technol.* **2022**, *293*, 121085. [[CrossRef](#)]
159. Mahdipoor, H.R.; Halladj, R.; Babakhani, E.G.; Amjad-Iranagh, S.; Ahari, J.S. Synthesis, characterization, and CO₂ adsorption properties of metal organic framework Fe-BDC. *RSC Adv.* **2021**, *11*, 5192–5203. [[CrossRef](#)]
160. Tovar, T.M.; Zhao, J.; Nunn, W.T.; Barton, H.F.; Peterson, G.W.; Parsons, G.N.; LeVan, M.D. Diffusion of CO₂ in large crystals of Cu-BTC MOF. *J. Am. Chem. Soc.* **2016**, *138*, 11449–11452. [[CrossRef](#)]
161. Yan, T.; Tong, M.; Yang, Q.; Liu, D.; Guo, Y.; Zhong, C. Large-scale simulations of CO₂ diffusion in metal-organic frameworks with open Cu sites. *Chin. J. Chem. Eng.* **2022**, *42*, 1–9. [[CrossRef](#)]
162. Jin, H.; Mo, K.; Wen, F.; Li, Y. Preparation and pervaporation performance of CAU-10-H MOF membranes. *J. Membr. Sci.* **2019**, *577*, 129–136. [[CrossRef](#)]
163. Liu, X.; Wang, C.; Wang, B.; Li, K. Novel organic-dehydration membranes prepared from zirconium metal-organic frameworks. *Adv. Funct. Mater.* **2017**, *27*, 1604311. [[CrossRef](#)]

164. Miyamoto, M.; Hori, K.; Goshima, T.; Takaya, N.; Oumi, Y.; Uemiya, S. An Organoselective Zirconium-Based Metal–Organic-Framework UiO-66 Membrane for Pervaporation. *Eur. J. Inorg. Chem.* **2017**, *2017*, 2094–2099. [[CrossRef](#)]
165. Dong, X.; Lin, Y. Synthesis of an organophilic ZIF-71 membrane for pervaporation solvent separation. *Chem. Commun.* **2013**, *49*, 1196–1198. [[CrossRef](#)]
166. Wu, F.; Lin, L.; Liu, H.; Wang, H.; Qiu, J.; Zhang, X. Synthesis of stable UiO-66 membranes for pervaporation separation of methanol/methyl tert-butyl ether mixtures by secondary growth. *J. Membr. Sci.* **2017**, *544*, 342–350. [[CrossRef](#)]
167. Wu, F.; Cao, Y.; Liu, H.; Zhang, X. High-performance UiO-66-NH₂ tubular membranes by zirconia-induced synthesis for desulfurization of model gasoline via pervaporation. *J. Membr. Sci.* **2018**, *556*, 54–65. [[CrossRef](#)]